J. Fluid Mech. (1992), *vol.* 235, *pp.* 285–317
Printed in Great Britain

The effects of gap width and dilute solution properties on the viscoelastic Taylor–Couette instability

By ERIC S. G. SHAQFEH[1], SUSAN J. MULLER[2] AND RONALD G. LARSON[2]

[1] Department of Chemical Engineering, Stanford University, Stanford, CA 94305-5025, USA
[2] AT&T Bell Laboratories, 600 Mountain Avenue, Murray Hill, NJ 07974, USA

(Received 16 October 1990 and in revised form 20 June 1991)

The effects of finite gap and various dilute solution properties on the previously studied purely elastic Taylor–Couette instability reported by Muller *et al.* (1989) and Larson *et al.* (1990) are investigated. The dilute solution properties which we consider are the ratio of the second to the first normal stress coefficient, Ψ_2/Ψ_1, and the ratio of the solvent to the polymer contribution to the shear viscosity, S. Linear stability predictions for the flow of an Oldroyd-B fluid are presented over a wide range of Deborah number, De, gap ratio, ϵ, and S. In addition, the Oldroyd-B model is modified to include second normal stress differences, and new stability predictions are presented for small negative and small positive Ψ_2/Ψ_1. Both the critical conditions and changes in the flow structure are presented. It is demonstrated that finite-gap effects are stabilizing even for relatively small gap ratios ($0 < \epsilon < 0.35$). Furthermore, it is shown that there are two possible flow structures which can be chosen near the onset of instability: a standing wave structure (i.e. radially propagating vortices) or a travelling wave (i.e. vortices propagating up or down the coaxial cylinders). However, the strength and both the axial and radial dimensions of these vortices depend markedly on the gap, with both dimensions decreasing as the gap ratio increases. Thus, the number of vortices filling the gap increases with the gap ratio.

In a second study, we show that the instability is sensitive to the presence of second normal stress differences. Positive second normal stress differences are shown to be destabilizing, while negative differences are strongly stabilizing. Furthermore, when both finite-gap effects and small negative second normal stress differences are included, the predicted gap dependence of the critical De is in good agreement with previous measurements on the flow of a dilute polyisobutylene solution. Finally, we present new measurements of the critical values of the De for a series of dilute, viscous polystyrene solutions, for which Ψ_2 was found to be near zero. We find that as the polymer concentration increases (and therefore S decreases) the critical Deborah number decreases, in qualitative agreement with the theoretical predictions.

1. Introduction

In previous publications (Muller, Larson & Shaqfeh 1989 and Larson, Shaqfeh & Muller 1990, hereinafter referred to as I and II respectively) we demonstrated that the low-Reynolds-number Taylor–Couette flow of a highly elastic fluid becomes unstable beyond a certain critical value of the Deborah number, De, which we

defined as the product of a characteristic polymer relaxation time and the shear rate in the Couette cell. Visualizations of the Taylor–Couette flow demonstrated that the plane shearing motion, associated with the flow at small values of De, is transformed into a cellular flow beyond a certain critical Deborah number. In addition, this critical value increases markedly as the ratio of the gap width to the radius of either cylinder decreases. In contrast with the transition first described by Taylor (1923), the instability of these highly elastic fluids occurs at very small values of the Taylor number, which is a measure of the ratio of centrifugal to viscous forces in the system. Thus, the instability is unrelated to inertial forces. This inference is reinforced by the observation that the transition occurs whether the inner or outer cylinder is rotated alone. In addition, the flow structure is characterized by a fairly small axial cell wavelength (i.e. apparently smaller than one gap width in length). Other characteristics of this transition include the observation that the cells are not completely regular and that time traces of the torque on the rotating cylinder at the transition show growing oscillations. All these experimental observations are reproducible with the same fluid, if the period following the transition is not too long. For fluids which had been subjected to the cellular flow for long periods of time, the viscoelastic properties of the solution showed evidence of flow-induced degradation. For details of these experiments, reference should be made to I and II.

Along with these experimental observations, we presented a linear stability analysis of the Taylor–Couette flow of an Oldroyd-B fluid in the limit of small gap. Note that this model has been shown to describe the steady flow of a restricted class of fluids known as Boger fluids (Boger 1977/78) even when the characteristic Deborah number is $O(1)$ and the fluids are thus highly elastic. A Boger fluid is a dilute solution of high-molecular-weight polymer dissolved in a viscous solvent. The high viscosity of the solvent produces a long characteristic relaxation time and ensures that the elastic forces remain important at flow rates low enough such that inertial effects remain small. We demonstrated that the Taylor–Couette flow of an Oldroyd-B fluid is, indeed, unstable past a critical value of the Deborah number even at vanishingly small Taylor number. The unstable mode is oscillatory (overstable) and characterized by an oscillation frequency which is of the order of the inverse characteristic polymer relaxation time. The mechanism for this instability involves the transfer of energy from the base flow to a fluctuation-induced radial normal stress. The predicted instability is therefore independent of centrifugal forces and occurs identically if either the inner or outer cylinder is rotated alone. A comparison of the theoretically predicted critical Deborah number with the experimental measurements showed fairly good agreement *if* the characteristic relaxation time used in the comparison is that obtained from transient shear flow experiments.

The purpose of the present communication is two-fold. First we wish to examine in greater detail the purely elastic instability discussed above. In this regard, we shall examine the structure of the flow predicted by the linear analysis. Therefore, we return to the stability eigenvalue problem presented previously, and examine the eigenmodes near the critical condition. In the limit of small gap, it is demonstrated that there are four such modes – two decaying and two growing – whose corresponding eigenvalues are complex conjugates as is characteristic of a standard Hopf bifurcation. Thus, if we restrict ourselves to the two most rapidly growing or critical modes, these represent travelling waves composed of tilted vortices which move in opposite directions along the axis of the Couette column. Another possible flow structure that could develop is a standing wave pattern produced by the sum of these two travelling modes; this corresponds to a radially propagating vortex

structure. In this pattern a vortex forms near the inner cylinder and simultaneously propagates and grows toward the outer cylinder. Typically, two vortices fill the channel at any particular time during the cycle. The standing wave structures are in good qualitative agreement with recent finite-element simulations of this flow (Northey, Brown & Armstrong 1989; Northey, Armstrong & Brown 1990).

After examining the structure of the flow predicted in the small-gap limit, we turn to the second purpose of this communication in which we examine two new effects on this purely elastic instability. In the first instance, we relax the small-gap assumption and examine finite-gap effects. Calculations are presented for gap ratios in the range $0 \leqslant \epsilon \leqslant 1$, but the range $0 \leqslant \epsilon \leqslant 0.25$ is emphasized. It is demonstrated that finite-gap effects are strong in this system. The flow is stabilized by these effects and the critical wavenumber is shifted to higher wavenumbers. However, the growing modes remain complex conjugates and both travelling wave and standing wave patterns can still be selected. Since the axial wavenumber has now increased, the travelling vortices are now of a higher aspect ratio. In addition, the radial wavenumber of the radially propagating standing wave structure also increases and thus a larger number of vortices fill the gap at any given time. The frequency of the overstable eigenfunctions is mildly increased. Finally, all of these effects are demonstrated to be strongest in the Maxwell fluid when the ratio of solvent to polymer viscosity, S, is identically zero. For larger values of S (in particular those values characteristic of Boger fluids used in our previous experiments (see I)) these effects are weaker though still significant. Thus, all the qualitative changes for Oldroyd-B fluids for arbitrary values of S can be predicted from the calculations involving the Maxwell fluid, but the effects are exaggerated in the latter calculations.

In a second study, we consider the addition of second normal stress differences (which are absent from the Oldroyd-B model) into our description of the fluid rheology. We recall that Giesekus (1966, 1982) in some of the earliest work on elastic instabilities demonstrated that these stress differences could destabilize Taylor–Couette flow at zero Reynolds number, but only if they were large and positive. He also demonstrated that positive second normal stress differences destabilize the stationary inertial Taylor mode even if they are small. In the present study, we find that small positive second normal stress differences also destabilize the purely elastic oscillatory mode and, moreover, negative second normal stress differences are stabilizing. Since experiments indicate that increasing the concentration of polymer in solution creates increasingly negative second normal stress differences (see Keentok *et al.* 1980; Larson 1988), we expect that the critical Deborah number can be increased such that the instability appears to vanish simply by changing the polymer concentration in the fluid. Indeed, it is suggested that this might be an alternative means of measuring second normal stresses in relatively dilute polymer solutions. Again, we find that this effect is strongest for the Maxwell fluid, and declines as one increases the value of S.

Our calculations which include finite-gap effects and small negative second normal stress differences are then compared to our previous experiments for the flow of a dilute viscous polyisobutylene solution. Good agreement is found between the theory and experiment, again, if the characteristic relaxation time chosen for comparison is that given by a stress relaxation experiment. This agreement includes the apparent stabilization (i.e. larger critical Deborah number) witnessed at very small gap which has not been explained heretofore via our small-gap theory. The presence of small negative second normal stresses is apparently a possible stabilizing factor.

In the final experimental section of the paper, we investigate the effect of

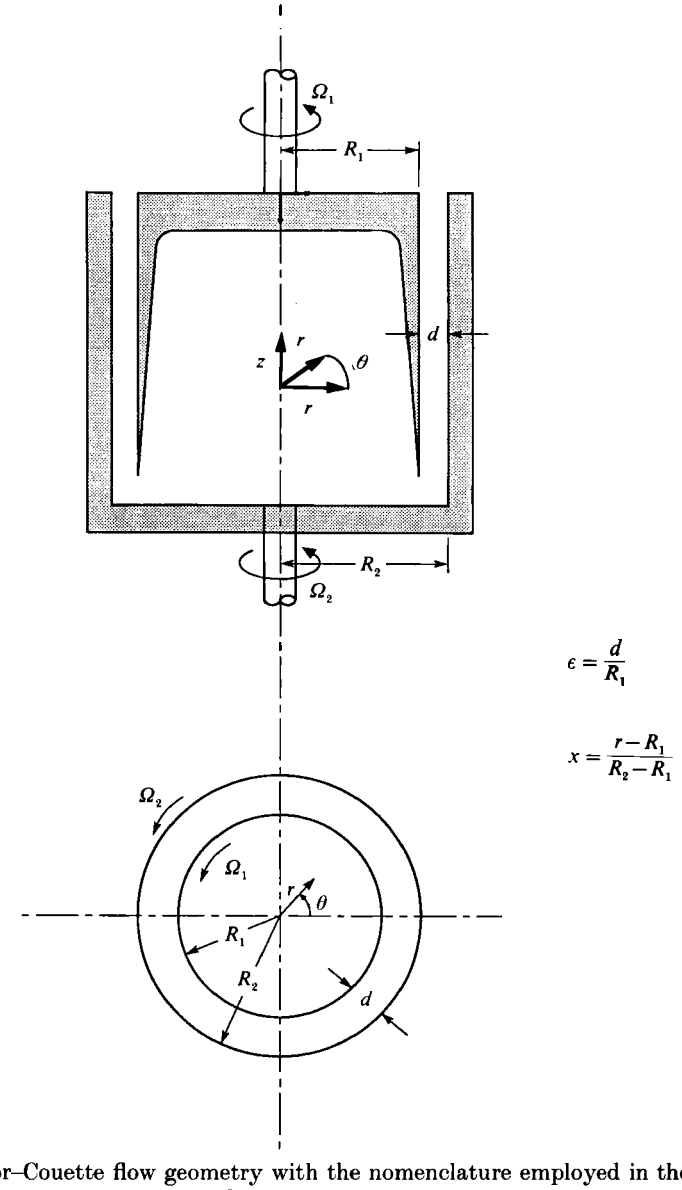

FIGURE 1. The Taylor–Couette flow geometry with the nomenclature employed in the present discussion.

increasing polymer concentration on the transition. Dilute polystyrene solutions are prepared at polymer concentrations ranging from 1000 to 6000 p.p.m. Rheological measurements of these solutions demonstrate that the shear viscosity and primary normal stress coefficient are slowly varying over a wide range of shear rate (small amounts of shear thinning are noticed only in the primary normal stress coefficients for shear rates in excess of 3 s^{-1}). Second normal stress differences were measured in these solutions and found to be vanishingly small within experimental error. Thus, only the ratio S changed appreciably among the different solutions; ranging from 1.0 to 6.3. Note that in our previous publications we have demonstrated that the stability criteria are identical for an Oldroyd-B fluid where $S = 1$ and for a Maxwell fluid. However, for values of $S > 1$ these criteria change significantly. Thus, the

experiments were planned to probe the behaviour of these instabilities in fluids ranging from one which was essentially a Maxwell fluid (in terms of its response to small fluctuations) to an Oldroyd-B fluid in which the solvent stress plays an important role in flow stability. Measured values of the critical Deborah number for the Taylor–Couette flow of these solutions demonstrated flow stabilization with increasing S (decreasing polymer concentration) in qualitative agreement with the theoretical predictions. However, the critical Deborah number was in general overpredicted for the flows at all polymer concentrations.

With this communication, we have begun the study of varying fluid rheology on the previously reported elastic instability. Since only relatively uncomplicated fluid rheologies have been considered, the theoretical and experimental parts of this area of research will be continued elsewhere.

2. Flow structures predicted from linear stability theory in the small-gap limit

In this section and in the Appendix, we return to the eigenvalue problem derived in II which governs the evolution of small disturbances in the Taylor–Couette flow of an Oldroyd-B fluid at zero Reynolds number. We recall in this context that the geometry of the flow and coordinate system are as pictured in figure 1, and that the base state flow, $\boldsymbol{v}^0$, is well known and equivalent to that found in a Newtonian fluid in the same device. In addition, the analytic expression for the base state stress tensor, τ^0 (which is composed of contributions from the polymeric material and the solvent in the Oldroyd-B model), is also available in II. We have previously considered the evolution of small normal mode disturbances applied to these base states, viz.

$$\tau = \tau^0 + \Gamma(x)\exp[-\mathrm{i}(\omega t - \alpha z)], \tag{2.1}$$

$$\boldsymbol{v} = \boldsymbol{v}^0 + \boldsymbol{V}(x)\exp[-\mathrm{i}(\omega t - \alpha z)], \tag{2.2}$$

where the amplitude functions Γ and $\boldsymbol{V}$ are functions of the gap variable, x, and where z is a coordinate running along the axis of the cylinders (cf. figure 1). In (2.1) and (2.2) as in all of the discussion which follows, all lengths have been made dimensionless with the gap width, d, and time with λ, the characteristic relaxation time of the polymer in the Oldroyd-B model. The characteristic complex frequency ω determines whether the perturbations will grow ($\mathrm{Im}(\omega) \equiv \omega_\mathrm{i} > 0$) or decay ($\omega_\mathrm{i} < 0$).

The eigenvalue problem whose solution determines ω in the limit of small gap ratio, $\epsilon \equiv d/R_1 \ll 1$, has been derived in II and is included for completeness:

$$U'''' - 2\alpha^2 U'' + \alpha^4 U + \alpha^3 \Lambda(\omega, \epsilon De^2, S)\, U' = 0, \tag{2.3a}$$

$$U = U' = 0, \quad x = 0, 1. \tag{2.3b}$$

In (2.3a, b), U is the amplitude function for the radial component of the perturbation velocity (or, in other words, the radial component of $\boldsymbol{V}$ in (2.2)) and the prime refers to differentiation with respect to x. Note that the eigenvalues Λ were found to be purely imaginary, so U is, in general, complex. The critical conditions for instability, critical wavenumber, and so forth have all been discussed elsewhere (see I, II and the Appendix). The critical parameter is $\epsilon^{\frac{1}{2}}De$. For given fluid properties and geometry, if we increase the cylinder rotation speed such that a certain critical value of this parameter is exceeded then a flow transition occurs through an oscillatory or overstable instability mode. In this discussion we concentrate on the possible flow

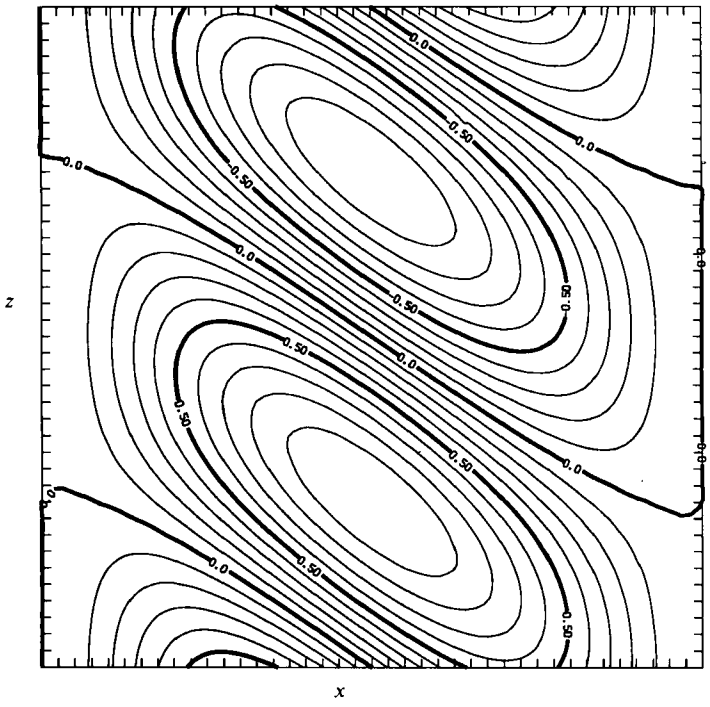

FIGURE 2. The streamlines in the (z, x)-plane corresponding to one of the two unstable eigenmodes for the Maxwell fluid. The flow is shown at an instant in time at the critical condition and is one full gap width across. Note that this mode propagates vertically upward with a velocity of one gap per polymer relaxation time, while the other unstable mode (i.e. the mirror image of this mode about the gap mid-plane) propagates downward with the same velocity.

structures which are predicted from the linear analysis at the onset of instability. If the bifurcation is supercritical, then one of these possible structures will be selected if we remain arbitrarily close to (but slightly past) the critical condition. Our discussion will again be a summary of the more detailed description available in the Appendix.

At the onset of instability in the elastic Taylor–Couette flow, there are two unstable modes which simultaneously grow in time. These modes are axisymmetric and composed of axially 'stacked' vortices which propagate with equal and opposite axial velocities. Thus, the base flow undergoes a Hopf bifurcation at the transition. These modes can most easily be portrayed via their streamlines in the (x, z)-plane. The complex stream function for the disturbance in the (x, z)-plane is

$$\Psi = \psi(x) \exp[\mathrm{i}(\alpha z - \omega t)], \quad \psi = \mathrm{i}U/\alpha. \tag{2.4a, b}$$

In figure 2 we have plotted the real stream function corresponding to one of these two critical growing eigenmodes for the Maxwell fluid ($S = 0$). These stream functions were numerically calculated by solving the system (2.3) using the orthogonal shooting method described in II. The mathematical expression for this stream function is

$$-\alpha \Psi_{\mathrm{u}}^{\mathrm{r}} = U^{\mathrm{i}} \cos(\alpha z - \omega^{\mathrm{r}} t) + U^{\mathrm{r}} \sin(\alpha z - \omega^{\mathrm{r}} t) \tag{2.5a}$$

$$= U^{\mathrm{i}} \cos 2\pi(Z - \tau) + U^{\mathrm{r}} \sin 2\pi(Z - \tau), \tag{2.5b}$$

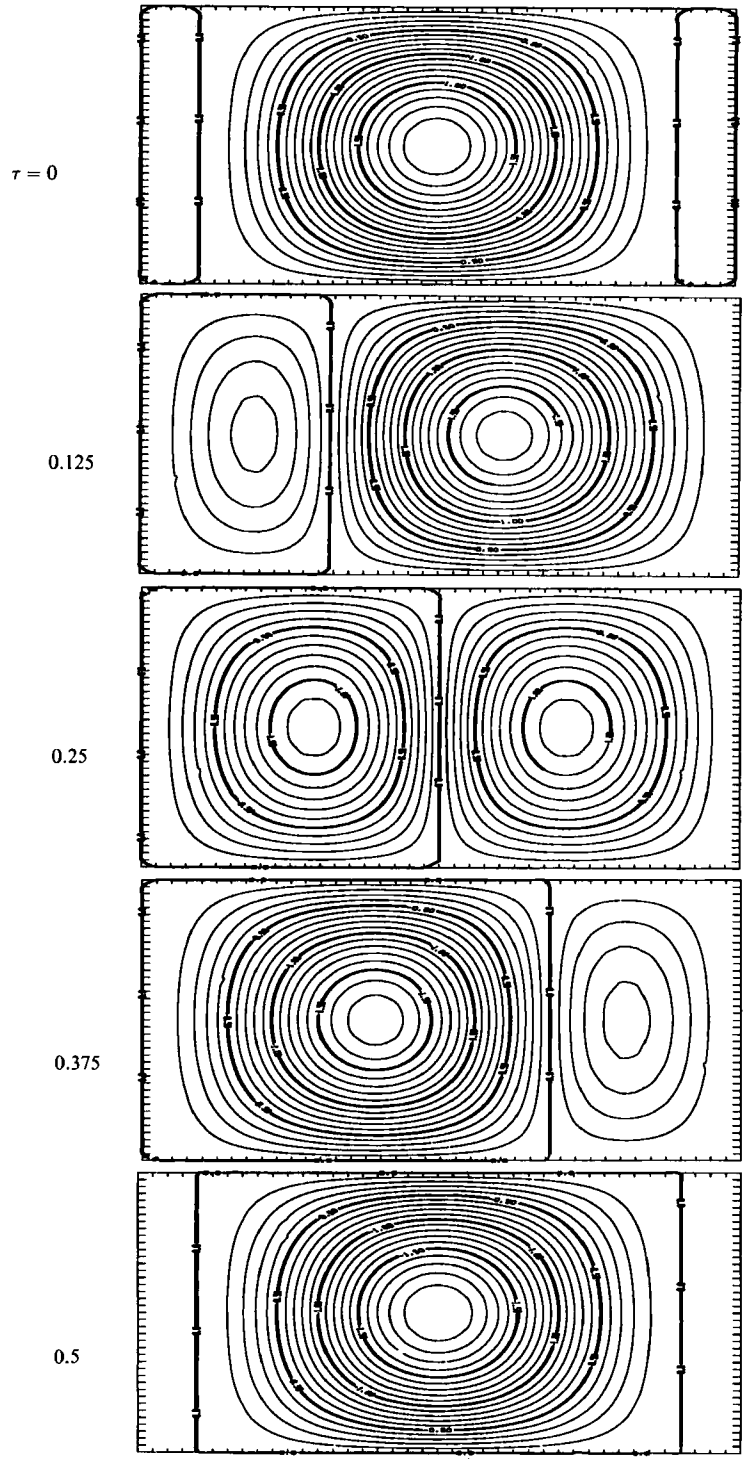

FIGURE 3. A time sequence of the standing wave pattern in the (z, x)-plane created by the two unstable eigenmodes of the Maxwell fluid at the critical condition. The sequence shows the growth of a vortex near the inner cylinder (left) and its propagation toward the outer cylinder (right) at a single fixed position along the axis of the cylinders. The time, τ, is measured in units of the characteristic oscillation period, $2\pi\lambda$, where λ is the polymer relaxation time.

where the superscripts 'r' and 'i' refer to the real and imaginary parts respectively and the subscript 'u' refers to the mode's upward motion toward the increasing values of z. In (2.5b), we have rescaled the z-coordinate and time, t, with the wavelength of the critical disturbance and the period of its oscillation respectively.

The vortex structure shown in this figure 2 is a travelling mode which modes 'up' the coaxial cylinders (i.e. in the direction in which the cells are tilted near the inner cylinder). There is an equivalent mirror-image structure which moves 'down' the coaxial cylinders, and whose constituent vortices are tilted downward near the inner cylinder (see the Appendix). The mode selection will depend on the symmetry of the initial perturbation, the axial end conditions applied to the Taylor–Couette cell, and the stability of these structures to external perturbations. In general, two possible qualitatively different structures can develop: one in which only travelling modes (either 'up' or 'down' the cylinders) exist and one in which the two equivalent modes will be present equally. In the latter case the resulting stream function will be produced by the sum of the two eigenfunctions, and will be a standing wave pattern given by the expression

$$-\alpha\Psi^{\mathrm{r}} = U^{\mathrm{i}}\cos 2\pi(Z-\tau)+U^{\mathrm{r}}\sin 2\pi(Z-\tau)-U^{\mathrm{i}}\cos 2\pi(Z+\tau)+U^{\mathrm{r}}\sin 2\pi(Z+\tau). \quad (2.6)$$

This flow is shown in figure 3, at various values of the dimensionless time, τ. The structure consists of radially propagating vortices, which form near the inner cylinder and grow radially, thus displacing vortices at larger values of the gap coordinate which coexist at any point in the cycle. In addition, at any point in the cycle as many as three vortices fill the gap; however, two of these are very weak and are positioned near the inner and outer cylinders respectively. More frequently, two vortices fill the channel. The cells in figures 2 and 3 are scaled with the correct relative dimensions (in gap width units) and thus we also see that the predicted cell structure consists of vortices which are slightly smaller than one half-gap in height (which is consistent with the critical wavenumber of 6.7 determined in II). The radially propagating vortex structure is in qualitative agreement with results from recent computer simulations of the fully nonlinear flow problem after the onset of the instability as presented by Northey *et al.* (1990). No axially propagating structures have been witnessed in any of the experiments or (to the author's knowledge) in any simulations of this purely elastic instability. More work clearly needs to be done before one can conclusively disregard the formation of travelling waves in this system. At present, however, linear analysis can reproduce the wave patterns which result from the fully nonlinear problem solution.

Note that although all of these calculations are for the Maxwell fluid, no qualitative changes in the linear structures were found for non-zero values of the viscosity ratio, S.

In all of the discussion and calculations presented in our previous publications, in the Appendix, and in the present section, we have concentrated on the small-gap limiting form of the stability problem. Previously, we derived the general eigenvalue problem which is valid for all gap ratios, and in the next section we examine the effects of finite-gap corrections on the flow stability.

3. Finite-gap effects in the linear stability for $0 \leqslant \epsilon \leqslant 1$

To examine finite-gap effects, we return to the general stability eigenvalue equations derived in Appendix A of II. These equations are quite general, encompassing inertial effects, second normal stress differences, arbitrary relative

rotation rate between the inner and outer cylinders, and so forth. Throughout the present study, we shall restrict our attention to the case of only the inner cylinder rotating, while keeping in mind that it is only in the limit of small gap that the stability is governed by the value of $(\Omega_1-\Omega_2)^2$, cf. (2.3). Thus, the stability characteristics for finite gap may differ significantly depending, for example, on whether we rotate the inner or outer cylinder alone, even if they are rotated at the same rate. In addition, for the analysis presented in this Section we shall neglect both inertial effects and second normal stress differences. The latter will be considered in §4.

With the aforementioned restrictions, the eigenvalue problem governing small disturbances in the Taylor–Couette flow of an Oldroyd-B fluid becomes

$$V''-\alpha^2 V = aU''+bU'+cU+dV'+eV, \tag{3.1a}$$

$$U''''-2\alpha^2U''+\alpha^4U = fU''''+gU''+hU'+kU+mV'+nV, \tag{3.1b}$$

$$U = U' = V = 0; \quad x = 0, 1, \tag{3.1c}$$

$$a = \frac{De}{(1+\epsilon x)^2}\frac{D^2}{D+S}, \quad b = \frac{\epsilon De}{(1+\epsilon x)^3}\frac{D(2-D)}{D+S}, \tag{3.1d, e}$$

$$c = \frac{-\epsilon^2 De}{(1+\epsilon x)^4}\frac{D(2-D)}{D+S}-\frac{\alpha^2 De}{(1+\epsilon x)^2}\frac{D^2}{D+S}, \tag{3.1f}$$

$$d = -\frac{\epsilon}{(1+\epsilon x)}, \quad e = \frac{\epsilon^2}{(1+\epsilon x)^2}, \quad f = -\frac{2\epsilon}{(1+\epsilon x)}, \quad g = \frac{3\epsilon^2}{(1+\epsilon x)^2}, \tag{3.1g–j}$$

$$h = -\frac{3\epsilon^3}{(1+\epsilon x)^3}+\frac{2\epsilon\alpha^2}{(1+\epsilon x)}-\frac{2\alpha^2\epsilon De^2}{(1+\epsilon x)^5}\frac{D^2(1+2D)}{D+S}, \tag{3.1k}$$

$$k = \frac{3\epsilon^4}{(1+\epsilon x)^4}-\frac{2\epsilon^2\alpha^2}{(1+\epsilon x)^2}-\frac{6\alpha^2\epsilon^2 De^2}{(1+\epsilon x)^6}\frac{D(2+D)}{D+S} \tag{3.1l}$$

$$m = \frac{2\alpha^2\epsilon De}{(1+\epsilon x)^3}\frac{D(1+D)}{D+S}, \quad n = -\frac{2\alpha^2\epsilon^2 De}{(1+\epsilon x)^4}\frac{D(1+D)}{D+S}. \tag{3.1m, n}$$

We recall in this context that V is the amplitude of the perturbation in the azimuthal velocity. In addition, the shear rate ceases to be constant across the gap beyond the small-gap limit and thus it is natural to define the Deborah number in (3.1) as

$$De = \frac{2\Omega_1\lambda(1+\epsilon)^2}{(1+\epsilon)^2-1}. \tag{3.2}$$

The right-hand side of (3.2) is equal to the product of the constant shear rate across the gap and the polymer relaxation time in the limit of small gap.

Note that the system defined by (3.1*a–n*) above is now sixth order in contrast to the fourth-order system defined by (2.3). Sixth-order eigenvalue systems also occur in the case of centrifugally driven instabilities (see Drazin & Reid 1981) and result from the curvilinear geometry. Thus, we see that, in general, the same is true of this elastically driven instability, but in the strict small-gap limit the system is degenerate and reduces to (2.3).

We have solved the system defined by (3.1*a–n*) over a wide range of parameter space, concentrating on modest gap ratios ($0 \leqslant \epsilon \leqslant 0.25$) because all of the experimental results described in §5 and in our previous publications involved these gap ratios. In addition, for somewhat larger gaps, it is extremely difficult to calculate

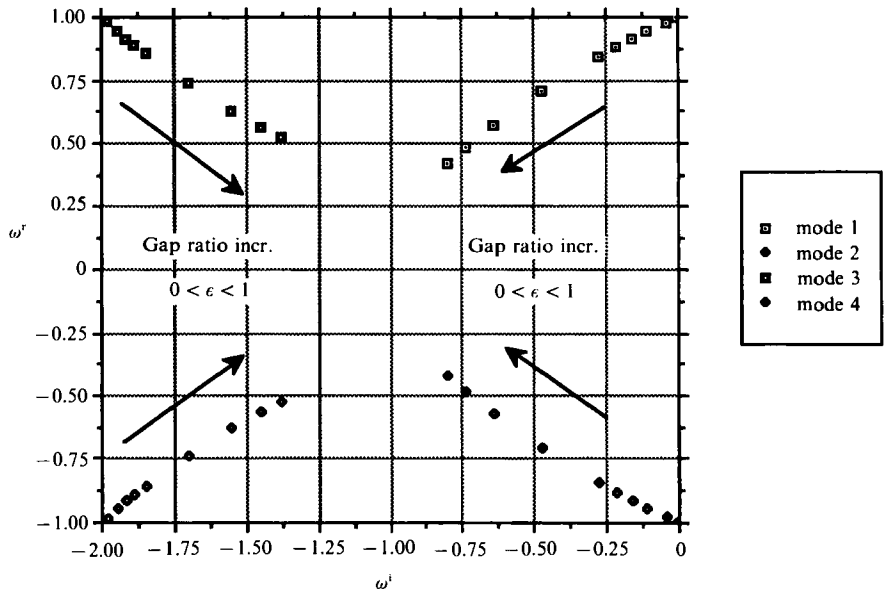

FIGURE 4. The movement of the eigenvalues in the complex ω-plane with the change in the gap ratio, ϵ, for the Maxwell fluid. Four of the infinite series of eigenvalues are shown at the parameters corresponding to the critical conditions in the limit $\epsilon \to 0$. As ϵ is increased the values move symmetrically toward the middle of the figure.

the critical condition for the instability (although it remains relatively easy to obtain neutral curves over a significant range of wavenumber) because the critical wavenumber increases sharply with the gap. These numerical difficulties will be discussed below.

3.1. *Maxwell fluid*, $S = 0$

We begin by considering the Maxwell fluid and its flow stability. Note, in this context, these are only model calculations and that we are not attempting to describe the flow behaviour of any specific viscoelastic fluid. However, we shall show that these calculations demonstrate all of the qualitative features of our more extensive calculations involving the more realistic Oldroyd-B model. In addition, it is shown in II that for $S = 1$ and in the small-gap limit, the behaviour of small perturbations is essentially identical to that of the Maxwell fluid theory. In §5, we will experimentally investigate instability growth in fluids where $S \approx 1$. Finally, the Maxwell fluid is used almost universally in large-scale computer simulations to predict the qualitative behaviour of viscoelastic flows. Thus, any instability in even these model problems is of great interest to those who are numerically simulating viscoelastic flows.

As is discussed in the Appendix, in the small-gap limit there are four modes at the critical condition whose eigenvalues are complex conjugates and which include the two critical modes that are unstable just beyond this condition. Figure 4 shows a typical trace in the complex plane of the eigenvalues of these four modes as the gap ratio, ϵ, is increased from zero to unity. The parameters have been chosen such that $\alpha = 6.7$ and $\epsilon^{\frac{1}{2}}De = 5.93$, which correspond to the critical condition in the small-gap limit. Thus, in figure 4, modes 1 and 2 are the critical modes which have zero imaginary eigenvalue as $\epsilon \to 0$, and modes 3 and 4 are the remaining decaying modes characterized by the same real frequencies as the growing ones. Note that even when the gap ratio is not vanishingly small the eigenvalues corresponding to the growing

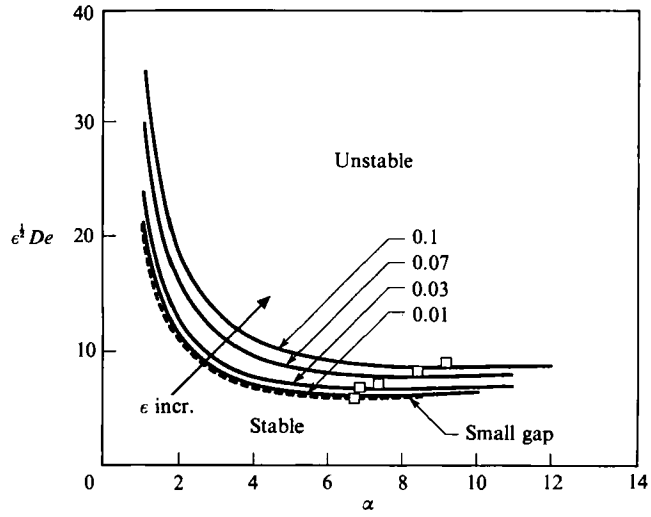

FIGURE 5. The change in the neutral stability curves for the elastic instability of the Taylor–Couette flow of the Maxwell fluid as the gap ratio increases. Plotted is the modified Deborah number, $\epsilon^{\frac{1}{2}}De$, *vs.* the wavenumber, α, for various values of the gap ratio, $0 \leqslant \epsilon \leqslant 0.1$.

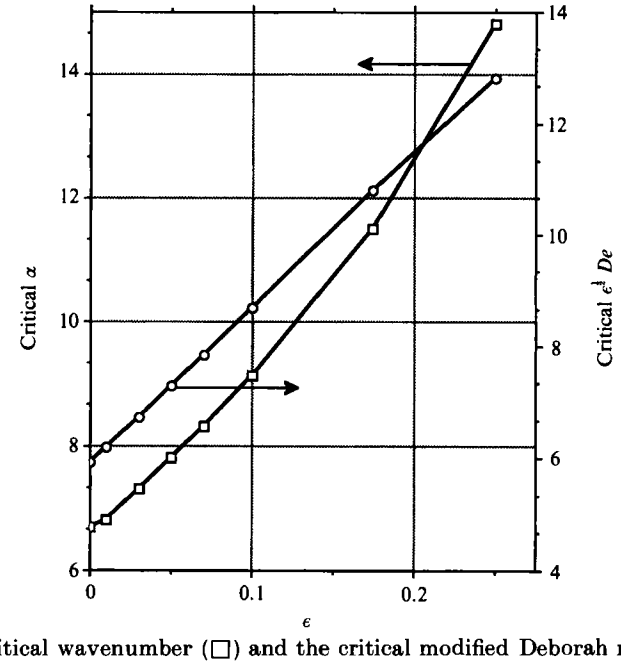

FIGURE 6. The critical wavenumber (□) and the critical modified Deborah number (○) *vs.* the gap ratio, ϵ, for the Maxwell fluid ($S = 0$).

and decaying modes respectively remain complex-conjugate pairs. This fact is not immediately apparent from the system (3.1), but, nevertheless, this was found for all eigensolutions at any value of the gap ratio. It follows that there exists a standing wave solution for each value of ϵ as is required by the axial symmetry of the physical system.

A summary of the neutral curves and critical conditions for the elastically driven instability of a Maxwell fluid at gap ratios $0 \leqslant \epsilon \leqslant 0.25$ is given in figures 5 and 6. In these figures we have referred to the product $\epsilon^{\frac{1}{2}}De$ as the *modified Deborah number*,

and we further note that this parameter plays a role analogous to the Taylor number in the centrifugally driven Newtonian instability. Figure 5 demonstrates that, in terms of $\epsilon^{\frac{1}{2}}De$, a finite-gap effects are monotonically stabilizing, generally increasing the value of $\epsilon^{\frac{1}{2}}De$ at which the flow becomes unstable to all wavelength perturbations. The stabilization is significant espccially near the critical conditions, which are summarized in figure 6 as a function of gap ratio. We note from this figure that both the critical modified Deborah number and the critical wavenumber increase strongly with increasing gap ratio – the latter most rapidly. (Note by contrast that the critical frequency increases with increasing gap ratio but only slightly over the same range of gap.) Thus, over a fairly small range in the gap ratio, $0 \leqslant \epsilon \leqslant 0.25$, the critical modified Deborah number increases from 5.932 (in the small-gap limit) to 12.81, while the critical wavenumber also increases from 6.7 to approximately 14.8. In the former case, the increase in the modified Deborah number is remarkably linear over the entire range of gap. This result suggests that, provided the linear analysis describes the ultimate evolution of any vortex structure in the flow of a Maxwell fluid, the gap ratio has a marked effect on the size of such vortices with the characteristic vortex dimension shrinking as the gap ratio increases.

The precipitous increase in the critical wavenumber with increasing gap ratio is in part responsible for our limiting these calculations to gap ratios smaller than 0.25. For larger gaps, although it was reasonably easy to obtain neutral curves including rather large values of the wave number, it became extremely difficult to obtain good numerical approximatiions to the critical condition because of the very large values of α involved. At these large values of the wavenumber, numerical accuracy in determining the Jacobian for our iteration scheme as well as in the eigensolution during integration and orthonormalization degenerates. We note in this context that under these conditions the eigenvalue problem was found to be extremely stiff. This 'stiffness' is associated with the increasingly complex and rapidly oscillating radial eigenfunctions which are found at large wavenumbers (cf. the discussion below). For obtaining precise values of these critical conditions at larger gaps, one must either use an alternative numerical method or employ a large-wavenumber analysis. We shall not pursue either of these in the present communication. We note that this numerical problem is somewhat less severe in our calculations for larger values of S, which we consider in the next subsection.

Although the effects of finite gap ratio are monotonically stabilizing in terms of the critical *modified* Deborah number, the critical Deborah number continues to decrease monotonically as the gap ratio increases. Of course this decrease is not nearly as rapid as predicted by the small-gap theory. We shall discuss this behaviour below, in our calculations for Oldroyd-B fluids and in comparison to measured critical values of the Deborah number.

Finally, we are interested in the change in the structure of the flow predicted by the linear analysis when the gap is increased from vanishingly small values. This is portrayed in figure 7, where we have plotted streamlines of the aforementioned standing wave structures (for $\tau = 0$) in the (z, x)-plane for various gap ratios. There are at least three important trends to note in analysing figure 7. First, and perhaps most obvious, the number of vortices filling the gap increases as the gap ratio increases. At a gap ratio of 0.25 as many as five vortices fill the channel at one time. Second, we note that the axial wavenumber at the critical condition has increased markedly and thus the axial wavelength of each cell decreases strongly with increasing gap. Finally, the strength of the vortices closest to the outer cylinder at first increases (as the vortices become of equal size) for $\epsilon \leqslant 1$ and then decreases with

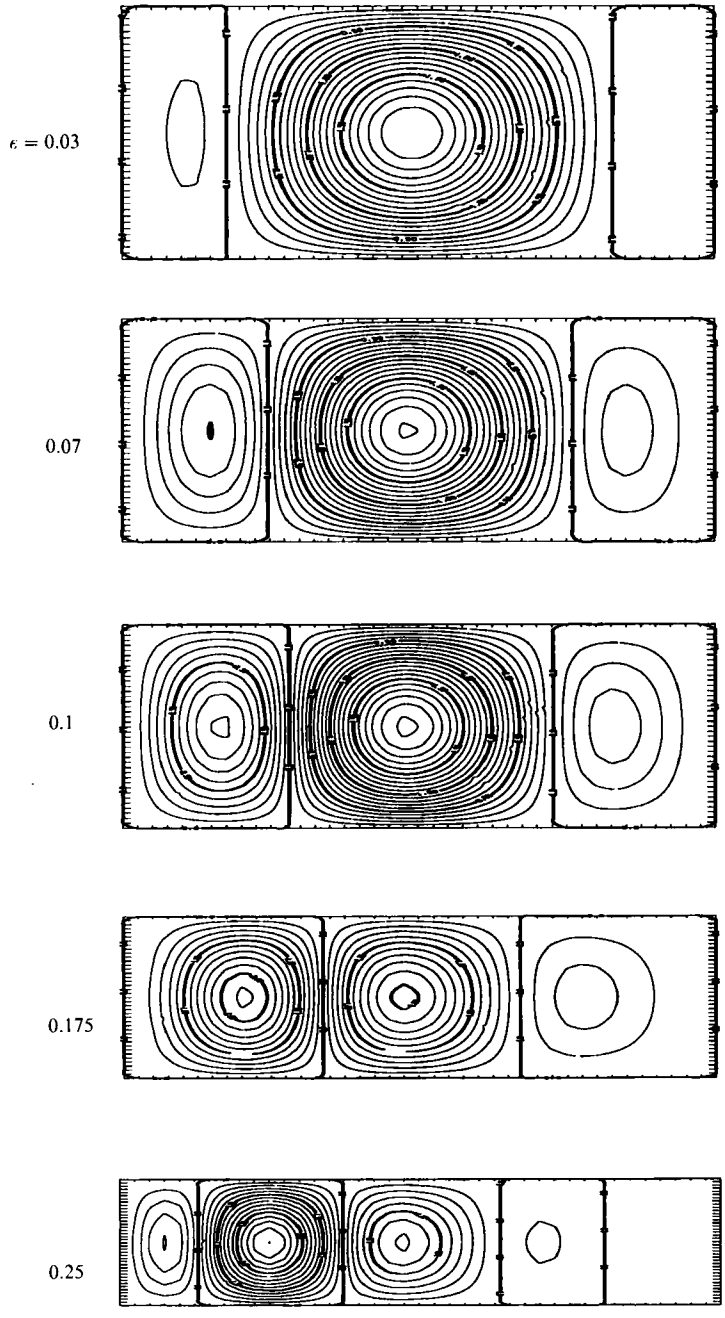

FIGURE 7. The disturbance streamlines for the standing wave pattern in the (z, x)-plane at $\tau = 0$ for the Maxwell fluid. Results are shown for one half an axial wavelength at the critical condition for various gap ratios $0 \leqslant \epsilon \leqslant 0.25$ (drawn to scale). Note the decrease in the size of the critical axial wavelength and the increase in the number of vortices which fill the gap.

increasing gap. These trends are reflected in the eigenfunctions as well. For the largest gap (0.25) there is almost no secondary flow near the outer cylinder (at $\tau = 0$). The decrease in the velocities near the outer cylinder is a reflection of the increase in the critical wavenumber. For these gaps the characteristic scale in the x-

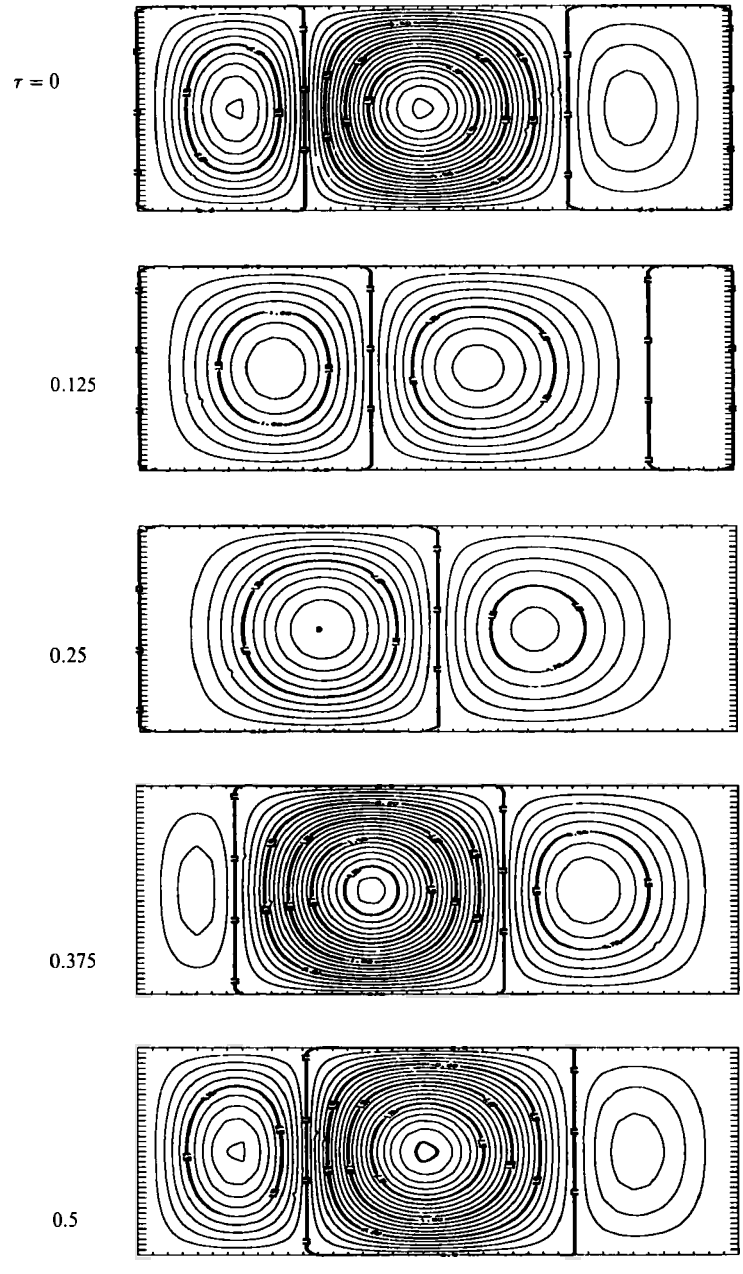

FIGURE 8. The disturbance streamlines for the standing wave pattern in the (z, x)-plane for the Maxwell fluid at $\epsilon = 0.1$. Results are shown at a fixed axial location but in a time series showing the propagation of the vortex from the inner cylinder (left) toward the outer cylinder (right).

coordinate is apparently no longer the gap width itself but is a function of the disturbance wavenumber. Thus, the calculations demonstrate that for larger gap ratios (and rotation of the inner cylinder only), we can expect disturbance vortices only relatively near the inner cylinder. To analyse this behaviour for larger gap ratios would require an analysis of very high wavenumbers which we shall not undertake here.

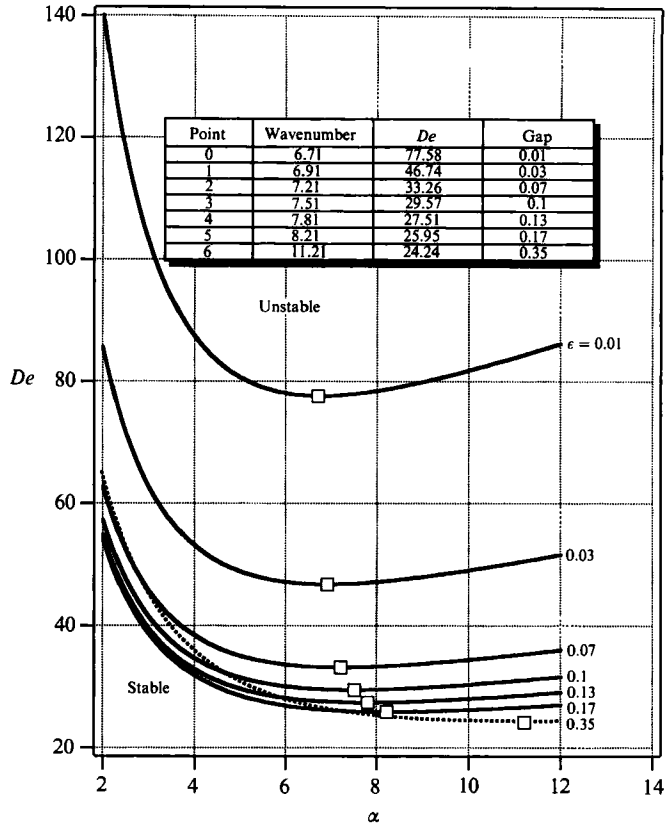

Point	Wavenumber	*De*	Gap
0	6.71	77.58	0.01
1	6.91	46.74	0.03
2	7.21	33.26	0.07
3	7.51	29.57	0.1
4	7.81	27.51	0.13
5	8.21	25.95	0.17
6	11.21	24.24	0.35

FIGURE 9. Neutral stability curves for an Oldroyd-B fluid (*De* vs. $\alpha, S = 3.75$) in Taylor–Couette flow for increasing gap ratio, $0 \leqslant \epsilon \leqslant 0.35$. ——, $\epsilon = 0.01$–0.17; ------, $\epsilon = 0.35$; □, critical conditions listed in the table.

In figure 8, for a gap ratio of 0.1, we show the time series of the vortices as they move through their characteristic oscillation. Again, these vortices propagate radially, but now the strengthening of the vortex as it approaches the centre of the gap is more marked, as is the decay of its strength as it continues to approach the outer wall. Note that for the gap ratio shown in this figure the strongest vortex at any particular time remains closest to the centre of the gap, while for the larger gap ratios (cf. figure 7) this is not the case. Thus, during propagation the vortex strengthens while staying relatively close to the inner cylinder, and then decays in strength through most of the gap as it approaches the outer wall.

As we mentioned previously, we have presented calculations in this Section for the Maxwell fluid primarily to indicate the qualitative effects of increasing the gap ratio on the elastic instability in Taylor–Couette flow and to guide large-scale numerical simulations of the instability which have concentrated on upper-convected Maxwell models. The experiments which are discussed in §5 involve Boger fluids, whose rheology is better described by the more general Oldroyd-B model where $S \geqslant 1$. In the next section then we shall briefly demonstrate the changes which occur in the predicted critical conditions when S is non-zero and finite-gap effects are considered.

Point	De	Gap	$\epsilon^{\frac{1}{2}}De$
0	71.1	0.02	12.31
1	35.25	0.067	9.124
2	23.94	0.129	8.6
3	24.292	0.14	9.09
4	23.88	0.167	9.76
5	26.39	0.25	13.19

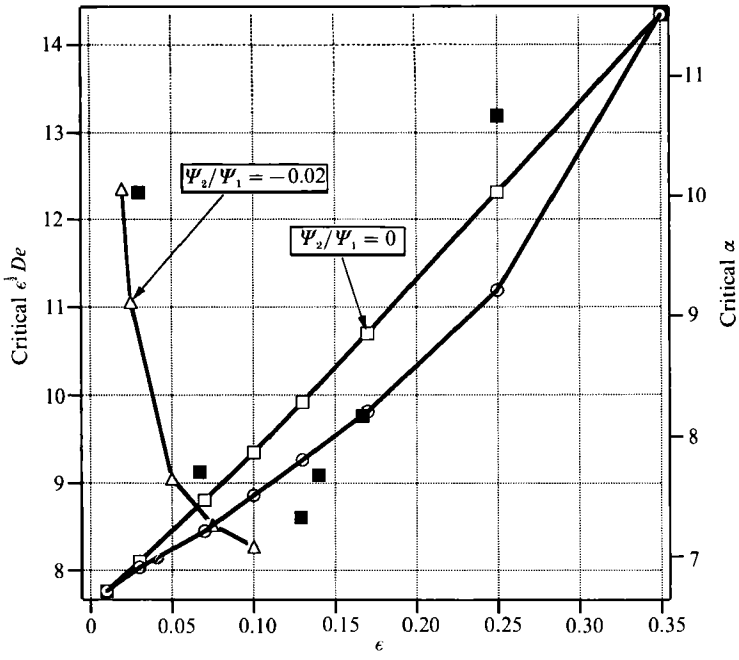

FIGURE 10. Summary of calculations and data for the Oldroyd-B fluid at $S = 3.75$. The critical modified Deborah number *vs.* the gap ratio. Calculations are included for zero second normal stress difference ($\Psi_2/\Psi_1 = 0$) with finite-gap effects included (—□—) and for negative second normal stress difference ($\Psi_2/\Psi_1 = -0.02$) in the limit of small gap (—△—). In the latter calculation the Oldroyd-B model was suitably modified as described in §3. Included are the measurements of the critical modified Deborah number reported by Muller *et al.* (1989) (—■—), which are also shown in the table. The critical wavenumber *vs.* the gap ratio is also shown (—○—).

3.2. *Oldroyd-B Fluid; $S \geqslant 1$*

Figures 9–11 summarize our initial investigation into finite-gap effects on the stability of elastic Taylor–Couette flow at non-zero values of the parameter S. All of these calculations are for $S = 3.75$ and gap ratios ranging from $0 \leqslant \epsilon \leqslant 0.35$. The value of S was chosen to correspond to the fluid used in our previous experiments (see I) and is fairly typical of dilute Boger fluids.

For the most part, these calculations provide the message that while the Maxwell fluid calculations indicate the qualitative effects of increasing the gap on the stability of the elastic flow, these effects are modified by the presence of a non-negligible solvent viscosity. This modification ranges from modest (in the case of predicting the critical Deborah number) to very significant (in predicting the critical wavenumber). Directly comparing these results to those for the Maxwell fluid (cf. figures 6 and 10) we find that the general trends are identical: as the gap ratio is increased, the critical modified Deborah number monotonically increases as does the critical wavenumber. However, the rate of change with increasing gap is slowed in the case of the Oldroyd-B fluid. In particular, the critical wavenumber increases more slowly with gap ratios

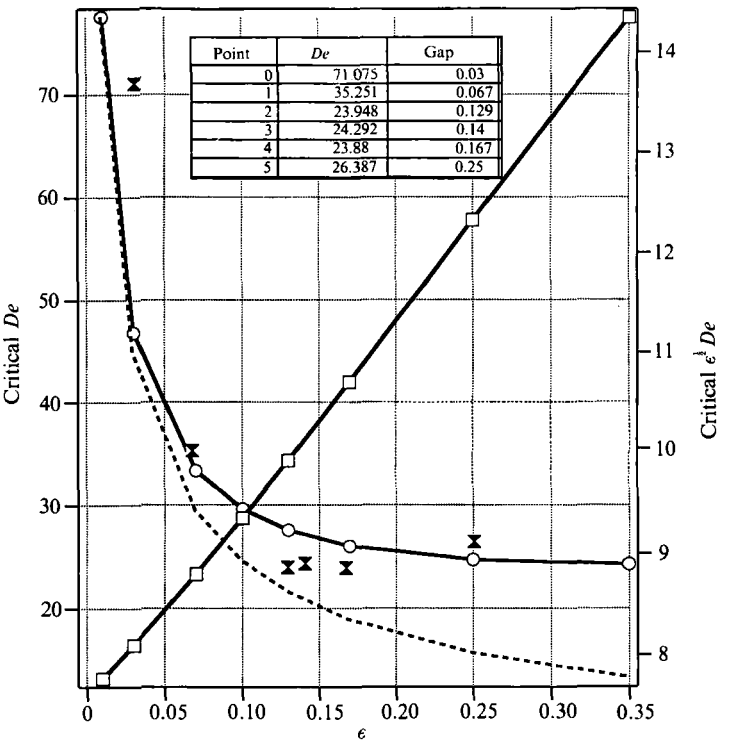

FIGURE 11. The critical Deborah number *vs.* the gap ratio as predicted by the linear stability calculations for the Taylor–Couette flow of an Oldroyd-B fluid (PIB) ($S = 3.75$). Theoretical predictions are shown in the limit of small gap (– – –) and for the theory including finite-gap effects (—○—, *De*; —□—, modified *De*). Included are the data from Muller *et al.* (1989) (⧗), which are also shown in the table.

than in the case of the Maxwell fluid (note that they are identical in the small-gap limit). Thus, we were able to extend our calculations up to a gap of 0.35. For larger gaps, although it was easy to obtain neutral curves, we could again not maintain sufficient numerical accuracy to unambiguously specify critical conditions because of the very large wavenumber at which the minima occur. In addition, from figures 9 and 11 we see that the critical Deborah number monotonically decreases with increasing gap and the neutral curves become increasingly 'flat' and thus are characterized by very shallow minima.

In figures 10 and 11, we also present the experimental data from I, which includes measurements of the critical conditions for the onset of instability. In figure 10 we present the data in terms of the modified Deborah number and in figure 11 we present the critical values of the Deborah number itself. Note that in both instances the Deborah number is based on an average shear rate for a finite gap flow (cf. (3.2)) rather that the limiting constant shear rate for small gap. We have used the latter in our previous publications (cf. II). In addition, we recall that in this comparison the characteristic relaxation time of the polymer is chosen to be that measured in a transient stress relaxation experiment, rather than that determined from steady rheological measurements. These two rclaxation times can differ by factors of 2–3 (see I, II, and §5). With these specifications then, for gap ratios greater than approximately 0.07, we find good agreement between the measured and predicted critical values of the Deborah number, which we note varies very slowly with

increasing gap ratio. We also find fairly good agreement in our predictions of the critical modified Deborah number which is more sensitive to errors in the measured gap ratio, shear rate, and fluid rheology (cf. figure 10). For gap ratios greater than 0.07, the trend in the measured critical modified Deborah number is in good accord with the theoretical predictions – each increasing approximately linearly with gap ratio. For small gap ratios, however, there appears to be a precipitous decrease in the modified Deborah number with increasing gap. This conclusion must be tempered by the fact that we only have a few data points available and the critical Deborah numbers are extremely large. Nevertheless, this trend is apparently not predicted by the finite-gap analysis. If our data accurately reflects this trend, then it becomes apparent that a different mechanism causes a large change in the stability characteristics of the flow at small gap ratios. Such a mechanism has been suggested by other work in the stability of elastic fluids, and we shall consider this mechanism in the next section.

4. The effect of second normal stress differences on the elastic instability

In our previous investigations of this elastic instability as described in I and II, the fluid rheology has been confined to the Oldroyd-B model. Indeed, rheological measurements presented in II and in §5 support this choice in describing the steady flow of dilute Boger fluids. One rheological property, however, which is both difficult to measure and is identically zero in the Oldroyd-B model is the second normal stress difference, N_2. In addition, there are strong implications from previous studies that N_2 may have a significant effect on the stability of an elastic flow even if it is very small relative to the primary normal stress difference, N_1. Giesekus (1972), in an early attempt to describe vortices in an elastic Taylor–Couette flow at small Taylor numbers, found a theoretical elastic instability which would occur if the ratio of secondary to primary normal stress coefficients (i.e. Ψ_2/Ψ_1, where Ψ_i is given by N_i divided by the square of the shear rate) times De^2 was $O(1)$ or greater. On the contrary, all measurements and theoretical predictions regarding Ψ_2/Ψ_1 show that this ratio is, in fact, small and negative or zero to within experimental error (Keentok *et al.* 1980; Larson 1988). For dilute Boger fluids, this ratio has been found to be particularly small, though we emphasize that accurate measurements are difficult to make. Molecular theory for dilute solutions predicts $|\Psi_2/\Psi_1| < 0.02$ at Deborah numbers of $O(10)$ (Larson 1988).

Although Giesekus found an instability which presumably has little physical consequence for elastic flows, he and others (Ginn & Denn 1969) demonstrated that the important parameter, which describes the effect of the second normal stresses on flow stability is the parameter $De^2\Psi_2/\Psi_1$, or in terms of the modified Deborah number, $(\epsilon De^2)\,\Psi_2/\Psi_1\,\epsilon$. Thus, although the ratio Ψ_2/Ψ_1 might be very small, as the gap ratio decreases the effects of the second normal stress coefficient will become important. It follows that our previous analysis needs to be modified to describe very small gap ratios.

In the general stability equations derived in II, second normal stress differences were added to the fluid rheology via a second polymer contribution to the stress which allowed the constitutive equation to include the second-order fluid as a special case. More general constitutive equations such as the 'Oldroyd-4 constant model' and the 'Oldroyd-8 constant model' allow for second normal stresses and for the continuous variation of Ψ_2/Ψ_1, but are much more complicated and involve a number of new parameters to describe the fluid rheology. Our choice in II is a special

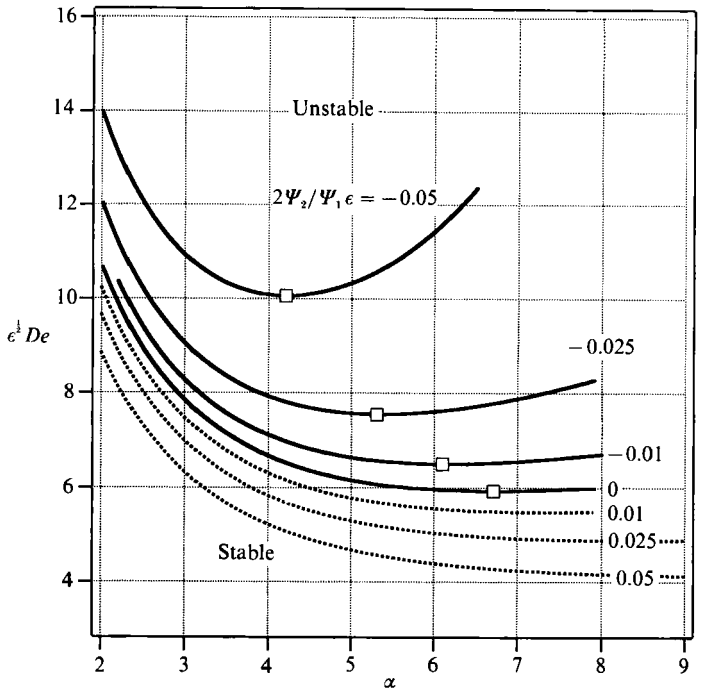

FIGURE 12. Neutral stability curves for the Taylor–Couette flow of a modified Maxwell fluid ($\epsilon^{\frac{1}{2}}De$ *vs.* α). The rheological model has been modified to include finite second normal stress differences and different stability bounds are pictured for $-0.05 \leqslant 2\Psi_2/\Psi_1\epsilon \leqslant 0.05$. ——, Negative second normal stress; ....., positive second normal stress.

case of the Oldroyd-8 constant model, which is simple and which we expect to predict qualitatively the effects of second normal stress differences in highly elastic fluids because of its relation to the second-order-fluid model. Therefore, from II, the small-gap limiting form of the new stability eigenvalue problem which includes the effects of second normal stresses is

$$U'''' - 2\alpha^2 U'' + \alpha^4 U + \epsilon De^2 \alpha^2 k U' + \alpha^2 \epsilon De^2 \psi \frac{D^2}{(D+S)^2}[U'' - \alpha^2 U] = 0 \qquad (4.1a)$$

$$U = U' = 0; \quad x = 0, 1, \qquad (4.1b)$$

$$k = 2\frac{D^2(D+S)(1+2D) - D^3(1+D)}{(D+S)^2}, \qquad (4.1c)$$

where $\psi = 2\Psi_2/\Psi_1\epsilon$, and we have assumed that the ratio Ψ_2/Ψ_1 is very small. This eigenvalue problem differs from the small-gap problem for the Oldroyd-B fluid only in the addition of the last term on the left-hand side of (4.1*a*). Note that we shall concentrate on the small-gap limit in this section because we anticipate, from our previous discussion, that it is in this limit that second normal stress differences will be most important.

In figure 12 we present neutral curves for the eigenvalue problem (4.1) for the Maxwell fluid, $S = 0$, over a range of small negative and small positive ψ. For negative values of ψ we find that the system is very strongly stabilized. Over the range $0 \leqslant \psi \leqslant -0.05$ the modified Deborah number increases by almost a factor of 2(!). For a gap ratio of 0.1, this range corresponds to $0 \leqslant \Psi_2/\Psi_1 \leqslant -0.0025$, thus

Point	Wavenumber	$\epsilon^{\frac{1}{2}}De$	ψ	
1	6.31	8.001	−0.25	
2	6.01	8.449	−0.5	
3	5.71	8.943	−0.75	
4	5.41	9.488	−1	
5	4.81	10.76	−1.5	

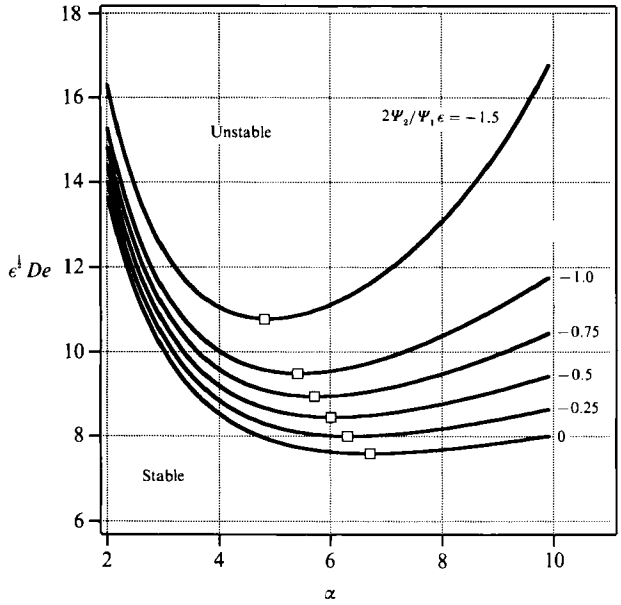

FIGURE 13. Neutral stability curves for the Taylor–Couette flow of a modified Oldroyd-B fluid ($\epsilon^{\frac{1}{2}}De$ *vs.* $\alpha, S = 3.75$). The rheological model has been modified to include finite second normal stress differences and different stability bounds are pictured for $-1.5 \leqslant 2\Psi_2/\Psi_1\epsilon \leqslant 0$. The critical conditions are shown in the table.

indicating a very strong sensitivity. Furthermore, we note that the critical wavenumber sharply decreases over the same range of ψ. Although these effects are quite dramatic we can expect from our previous experience with finite-gap effects that while the Maxwell fluid calculations indicate qualitative trends, the corresponding results for the Oldroyd-B fluid at values of S consistent with experimentally realizable fluids will be substantially modified. Indeed, this is again the case as we indicate in figure 13, where we present neutral curves for the Oldroyd-B fluid for $S = 3.75$. Clearly, although the effects of second normal stresses are stabilizing the effect is not nearly as dramatic; for example, the critical modified Deborah number increases by less than 50% for values of ψ as large as -1.5. In addition, the critical wavenumber decreases as ψ becomes more negative, but the decrease is much more modest.

The conclusions of this study are summarized in figure 10. Since the important parameter which describes the stabilizing effect of second normal stresses on the flow is $\psi = 2\Psi_2/\Psi_1\epsilon$, it follows that if the fluid rheology is kept constant but the gap is decreased, then ultimately the second normal stress difference, if not identically zero, will dominate the development of an instability in this system. In figure 10 we have added to the finite-gap calculations (which excluded all second normal stress differences), our small-gap results for $\Psi_2/\Psi_1 = -0.02$ over the range $0.02 \leqslant \epsilon \leqslant 0.1$. The value of the ratio Ψ_2/Ψ_1 is consistent with the range of theoretical predictions and experimental measurements for dilute polymer solutions (Keentok *et al.* 1980; Larson 1988). It has been chosen simply to illustrate that these stresses are strongly

stabilizing at small values of the gap ratio, but are negligible at larger gaps. This trend is consistent with our experimental measurements in the small-gap range. We have not attempted to make a quantitative comparison because no measurements of the second normal stress coefficient characterizing the PIB fluid used in our previous experiments were made. In fact, since the error in all available techniques for measuring Ψ_2/Ψ_1 is at least as great as ± 0.01 (see Magda *et al.* 1991), no quantitative confirmation of the effect of Ψ_2/Ψ_1 at small gap ratios would be possible, even if the relevant rheological measurements were available. A qualitative comparison is possible however if a series of fluids can be prepared in which $-\Psi_2/\Psi_1$ ranges from 0 to 0.1 or higher. Since $-\Psi_2/\Psi_1$ has been found to increase with polymer concentration and to exceed 0.1 for very concentrated solutions (Keentok *et al.* 1980) such a study would be possible by simply increasing the polymer concentration in solution. Finally, in this context, we note that, to our knowledge, no non-inertial instabilities have been reported in the Taylor–Couette flow of concentrated polymer solutions, which might be in part due to the relatively large values of $-\Psi_2/\Psi_1$ in these fluids.

5. Experiments

5.1. *Fluid preparation*

As remarked previously, our initial studies of the Taylor–Couette flow of a dilute polymer solution considered a single polyisobutylene (PIB)/polybutene solution. The preparation and rheological characterization of this solution, flow visualization of the Taylor–Couette transition, and the effect of gap on the critical Deborah number for the transition are described in I and II.

In the present experiments, we have chosen a different fluid system to investigate the effect of increasing polymer concentration on the Taylor–Couette transition. Like the earlier solutions, the new ones are 'Boger fluids' i.e. a small amount of a high-molecular-weight polymer was dissolved in a viscous, Newtonian solvent. The Newtonian 'solvent' was itself a solution containing 28% by weight of a monodisperse, low-molecular-weight ($M_w/M_n = 1.06$, $M_w \approx 47\,500$) polystyrene (PS) dissolved in diocytl phthalate (DOP). Dioctyl phthalate is a theta solvent for PS at 22 °C (Berry 1967) and at this concentration, the low-molecular-weight PS should be unentangled. Thus, this solution is Newtonian at the shear rates investigated, and can be considered a solvent for the high-molecular-weight species, which was a nearly monodisperse ($M_w/M_n = 1.20$) polystyrene with $M_w \approx 2.0 \times 10^7$. Both the low- and high-molecular-weight polymers were obtained from Pressure Chemical Company.

The PS/DOP solvent and solutions containing 1000, 2000, 4000, and 6000 p.p.m. of the $2.0 \times 10^7 M_w$ PS in the PS/DOP solvent were all prepared by the same procedure. The high- and low-molecular-weight PS were first dissolved in carbon disulphide, a good solvent with a low boiling point, and then DOP was added to produce a homogeneous mixture. The resulting solutions were then heated under vacuum at 40 °C to remove the carbon disulphide.

5.2. *Rheological characterization*

The solutions were characterized in steady shear and in cessation of steady shear flow on a Rheometrics System IV Mechanical Spectrometer using cone and plate fixtures. In all of the experiments, the temperature was maintained at 22.0 ± 0.5 °C by an existing convection oven. This degree of temperature control (i.e. ± 0.5 °C) introduces

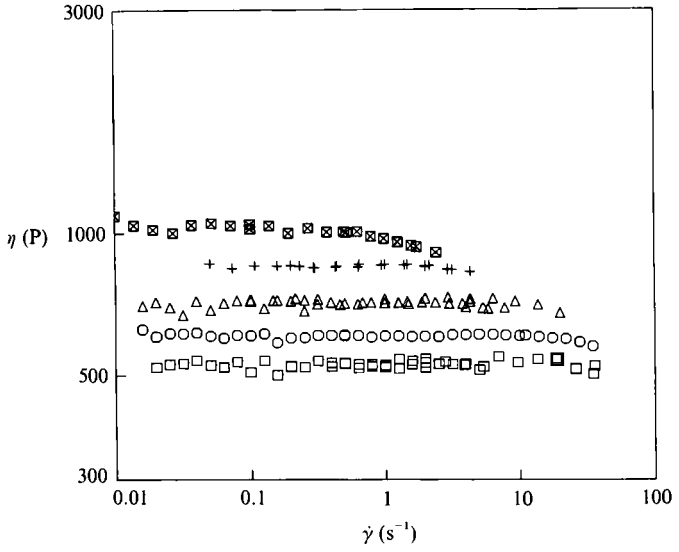

FIGURE 14. The steady shear viscosity as a function of shear rate for the PS/DOP solvent and solutions containing 1000, 2000, 4000, and 6000 p.p.m. high-molecular-weight PS.

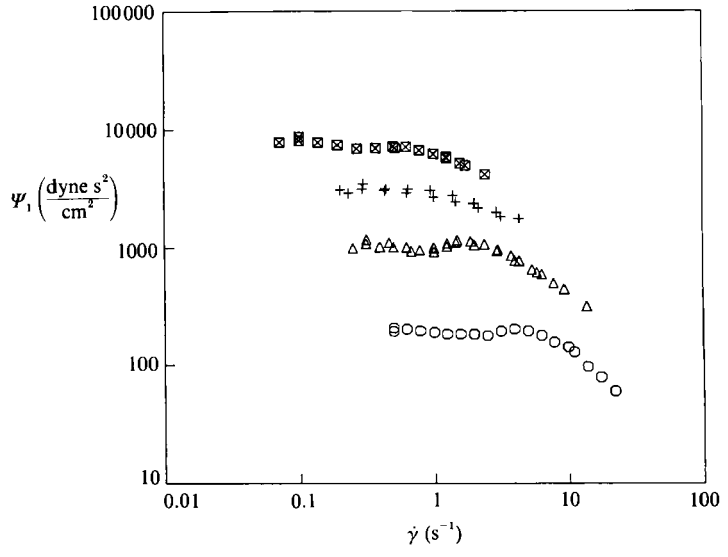

FIGURE 15. The first normal stress coefficient as a function of shear rate for the PS/DOP solvent and solutions containing 1000, 2000, 4000, and 6000 p.p.m. high-molecular-weight PS.

an uncertainty of not more than $\pm 5\%$ in the measured viscosities and first normal stress differences. Better control of the temperature would have required a major modification of the rheometer and the test cells, which seemed unwarranted for the present study.

The steady shear viscosity η and first normal stress coefficient Ψ_1 for the five solutions are shown as a function of shear rate in figures 14 and 15, respectively. Note that the PS/DOP solvent displayed no shear thinning and no measurable normal stresses for shear rates as high as 30.0 s^{-1}. For the solution containing the lowest

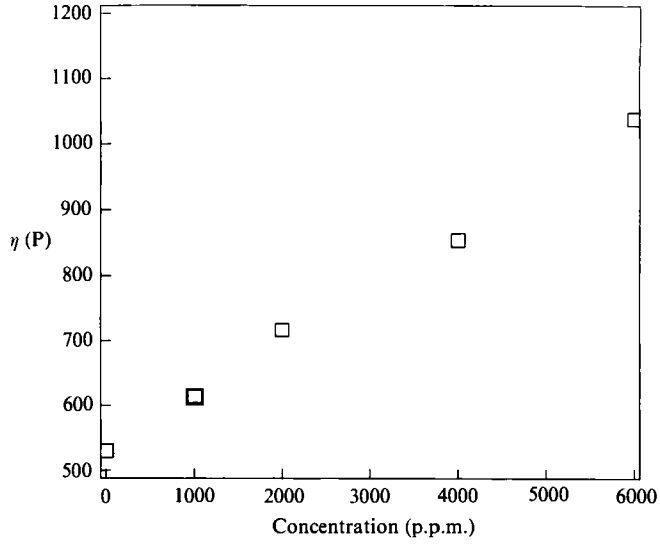

FIGURE 16. The solution viscosity at vanishing shear rate as a function of the concentration of high-molecular-weight PS.

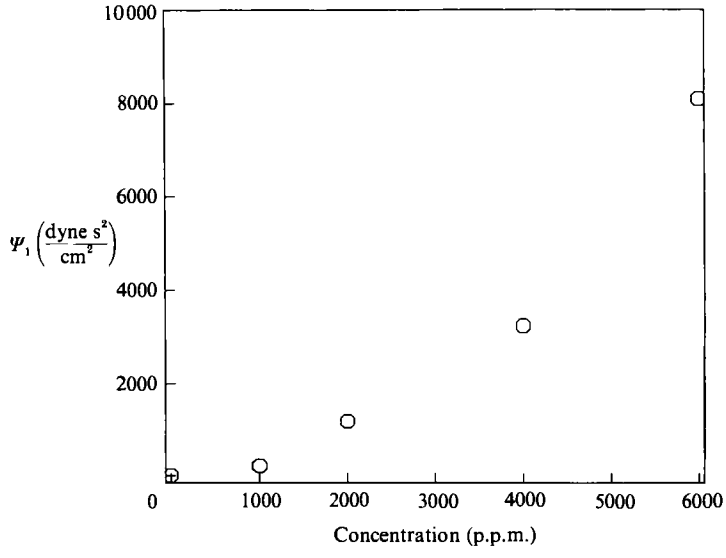

FIGURE 17. The first normal stress coefficient at vanishing shear rate as a function of the concentration of high-molecular-weight PS.

concentration of the high-molecular-weight PS (i.e. 1000 p.p.m.), shear thinning is apparent only in the first normal stress coefficient. As the concentration of high-molecular-weight PS increases, the viscosity and first normal stress coefficient increase and the shear rate at which shear thinning first appears decrease. The zero shear rate viscosity and first normal stress coefficient are shown as functions of concentration in figures 16 and 17. The ratio of the solvent to the polymeric contribution to the viscosity, $S = \eta_s/\eta_p$, and an Oldroyd-B relaxation time $\lambda = \Psi_{10}/2\eta_p$ can also be determined from these data. This information is summarized in the first five columns of table 1.

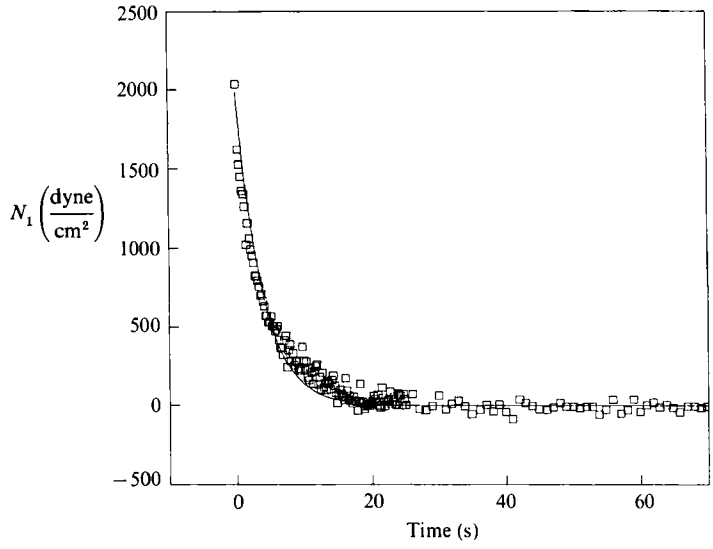

FIGURE 18. The decay of the primary normal stress as a function of time on the cessation of steady shear flow. The flow was stopped at time $t = 0$. The symbols represent the measurements, the solid curve is the least-squares fit to the single exponential decay predicted by the Oldroyd-B model.

Concentration (p.p.m.)	η_0 (P)	Ψ_{10} $\frac{\text{dyne s}^2}{\text{cm}^2}$	$S = \frac{\eta_s}{\eta_p}$	$\lambda_s = \frac{\Psi_{10}}{2\eta_p}$ (s)	λ_t (from $N_1(t)$) (s)
0	539.0	0		0	0
1000	614.0	213.0	6.3	1.27	3.75
2000	717.0	1184.0	2.8	3.17	9.50
4000	855.0	3232.0	1.6	4.97	12.2
6000	1038.0	8088.0	1.0	7.96	18.9

TABLE 1. Concentration dependence of rheological properties

In addition, the decay of normal stress following the cessation of steady shear flow was measured for each fluid. This was done at shear rates below those at which the primary normal stress coefficient shows shear thinning in steady shear flow. The measurements were then fit to the single exponential decay predicted by the Oldroyd-B equation; an example of the measurement and the least-squares fit is shown in figure 18. This relaxation time is reported in column 6 of table 1. For the lowest-concentration fluids, this transient measure of the relaxation time is a factor of nearly three higher than the relaxation time determined from the steady shear properties. For the more concentrated fluids, the ratio of these relaxation times decreases slightly to 2.4. A discrepancy between these two measures of the relaxation time was previously noted with the PIB/polybutene Boger fluid in I and II; it is indicative of the distribution of relaxation times which is present in the real fluid. A constitutive model containing a spectrum of relaxation times would thus provide a more accurate description of the real fluid than the (single relaxation time) Oldroyd-B model. However, the Oldroyd-B model provides a simple approximation that appears to capture many of the qualitative features of the real fluid behaviour

through a range of shear rates in which Ψ_1 and η are approximately constant. In fact, our recent analysis (see Larson, Muller & Shaqfeh 1991) of this instability using constitutive models which include a spectrum of relaxation times indicates that none of the qualitative features of the transition are modified by the spectrum. In addition, we demonstrate that the spectrum gives only a slightly better quantitative comparison with our experimentally measured critical conditions. In this context, we note that Quinzani *et al.* (1991) have discussed the rheology of Boger fluids in great detail and have remarked on the limitations of characterizing the fluid rheology with a multimode Oldroyd-B model.

Finally, the second normal stress coefficient was measured to be vanishingly small (i.e. $\Psi_2/\Psi_1 = 0.0 \pm 0.01$) for each of these solutions in an independent set of experiments. These data are reported elsewhere (Magda *et al.* 1990; Lee *et al.* 1991). Although these measurements are notoriously difficult, the techniques employed in this particular case were designed to render the highest degree of accuracy in evaluating Ψ_2 and thus the small experimental error. We can, therefore, with confidence ignore the effects of second normal stresses in these fluids, which we recall are most often stabilizing according to our theoretical predictions. All of the rheological data suggest that below some shear rate (at which the first normal stresses begin to shear-thin), all the fluids behave essentially like Oldroyd-B fluids; hence, S and λ may be varied considerably by varying the concentration of the high-molecular-weight PS without otherwise affecting the rheology. It is the change in the stability characteristics with the variation of the parameters S and λ which we wish to investigate in the experiments described below.

5.3. *Taylor–Couette experiments*

The Rheometrics System IV was used with a custom-made Taylor–Couette cell to study the behaviour of the PS/PS/DOP test fluids in flow between concentric cylinders. The steady motor of the System IV was used to impose a constant rotation speed on the inner cylinder of the Couette device; the torque on the stationary outer cylinder was measured using a Rheometric strain gauge transducer. The base of the inner cylinder was recessed so that a sharp edge was left around the circumference; as a result air was trapped beneath the inner cylinder. There was a free surface at the top of the cell. The radii of the inner and outer cylinders were 14.5 and 16.0 mm, respectively, which gives a gap ratio ϵ of 0.10. The cell was typically filled to a height of 40 mm so that the height-to-gap ratio was 27. The Couette cell was enclosed in the System IV convection oven; a temperature controller maintained the temperature at 22.0 ± 0.5 °C throughout the experiments. As in our previous studies in I and II, the Taylor number was less than 10^{-6} (Reynolds number less than 10^{-2}) throughout these experiments.

A series of experiments was conducted as follows: the inner cylinder was brought impulsively from rest to a given rotation rate which was maintained for long times (relative to any fluid timescale) and the torque on the outer cylinder was measured as a function of time. At low shear rates, the torque reaches a plateau value within a few seconds and remains constant for as long as the fluid is sheared. This low-shear-rate torque plateau is always consistent with a steady shearing flow between the cylinders where the fluid viscosity is known from the cone and plate measurements. As with the PIB/polybutene solution, however, each of the PS/PS/DOP solutions displayed a critical shear rate above which the torque on the outer cylinder departed from that consistent with a purely azimuthal steady shearing flow between the cylinders. These critical shear rates are given in table 2. Note that in each case, the

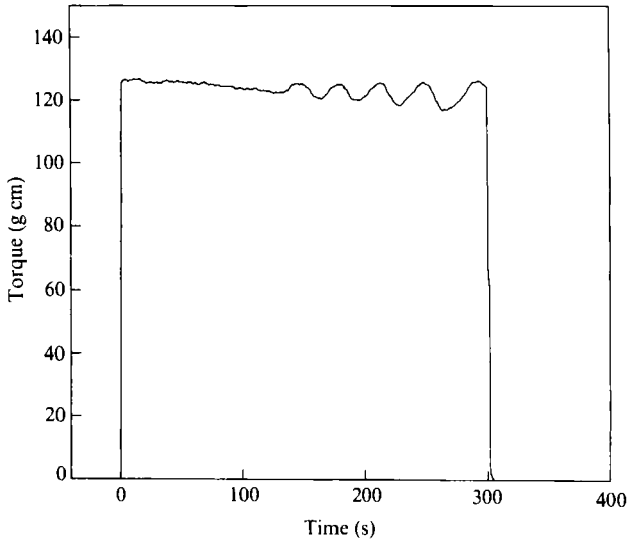

FIGURE 19. The torque as a function of time for the Taylor–Couette flow of the 1000 p.p.m. solution. The shear rate $\dot{\gamma}$ was zero for times $t < 0$ and was $\dot{\gamma} = 7.8\ \mathrm{s}^{-1}$ for $0 < t < 300$ s.

Concentration (p.p.m.)	$S = \frac{\eta_s}{\eta_p}$	$\dot{\gamma}_c$ (s^{-1})	De_c from λ_s	De_c from λ_t	De_c Theory
0		>46			
1000	6.3	7.4	9.4	28	35.2
2000	2.8	2.8	8.9	27	27.8
4000	1.6	1.4	7.0	17	24.7
6000	1.0	0.9	7.2	17	24.3

TABLE 2. Concentration dependence of critical conditions

critical shear rate in Taylor–Couette flow is reached before any significant shear-thinning in the normal stresses is anticipated based on the cone and plate data in figure 16. These critical shear rates, expressed in terms of Deborah numbers (as defined by (3.2)), are given in columns 4 and 5 of table 2. The two different values for the Deborah number reflect the two different measures of the relaxation time. It is significant that if one takes the longer of the two relaxation times as the appropriate one, the critical Deborah number measured experimentally is in fairly good agreement with the theoretical value for all of the PS/PS/DOP solutions, although we generally overpredict the critical Deborah number (cf. table 2). The longer relaxation time also gave the appropriate critical Deborah number for the polyisobutylene solution (see I and II). These experiments on two completely different fluids, which include a concentration series for the PS solutions give us confidence in the universality of the instability in dilute solutions and in our qualitative prediction of the critical Deborah number for onset. In this context, we also mention that Laun & Hingmann (1990) have recently witnessed the elastic Taylor–Couette transition in their study of yet another Boger fluid – the fluid M1.

A typical torque trace for the lowest-concentration PS solution subjected to a shear rate just above the critical value is shown in figure 19. The initial value of the torque is consistent with a steady azimuthal flow between the cylinders; it decreases

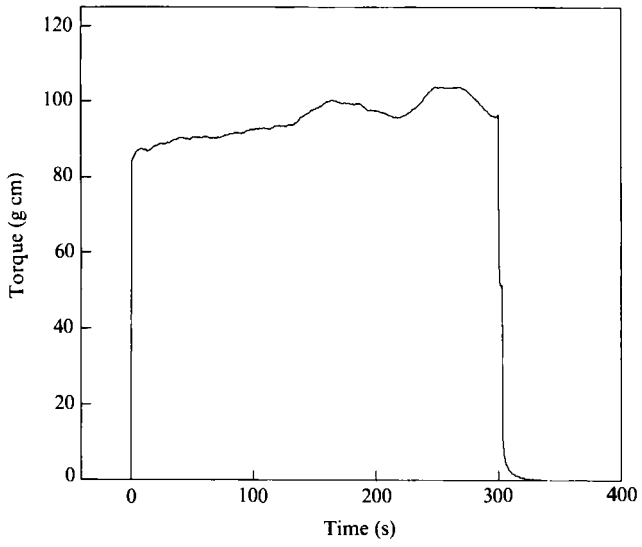

FIGURE 20. The torque as a function of time for the Taylor–Couette flow of the 2000 p.p.m. solution. The shear rate $\dot{\gamma}$ was zero for times $t < 0$ and was $\dot{\gamma} = 3.9\ \mathrm{s}^{-1}$ for $0 < t < 300$ s.

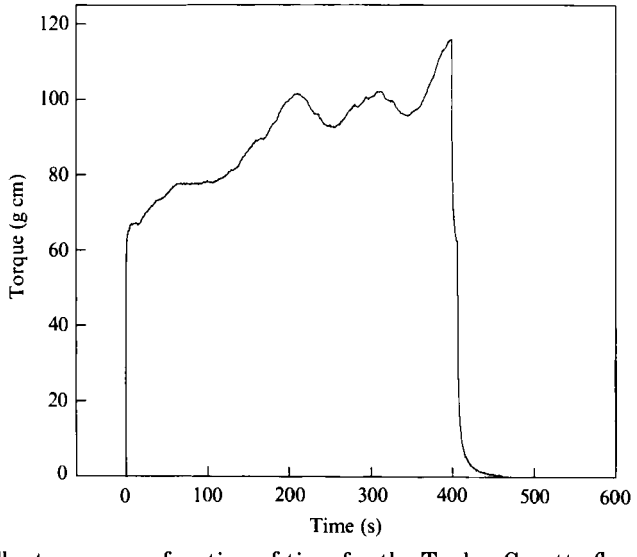

FIGURE 21. The torque as a function of time for the Taylor–Couette flow of the 4000 p.p.m. solution. The shear rate $\dot{\gamma}$ was zero for times $t < 0$ and was $\dot{\gamma} = 2.8\ \mathrm{s}^{-1}$ for $0 < t < 400$ s.

slightly over approximately 140 s and then becomes clearly time periodic with a period of roughly 33 s. This compared favourably to the predicted period of 28.8 s that one calculates for the oscillation of the streamline pattern. The amplitude of the torque oscillation continues to increase for the next 160 s until the imposed rotation is halted.

For the more concentrated solutions, the mean amplitude of the torque increased significantly (relative to the torque consistent with a steady shearing flow) at shear rates above the critical. This is evident in comparing figures 19–22. Evidence of the time periodicity is much less clear in the flows of these more concentrated solutions; however, there still appear to be oscillations in the torque amplitude with a period which is now substantially increased over that portrayed in figure 18. The period

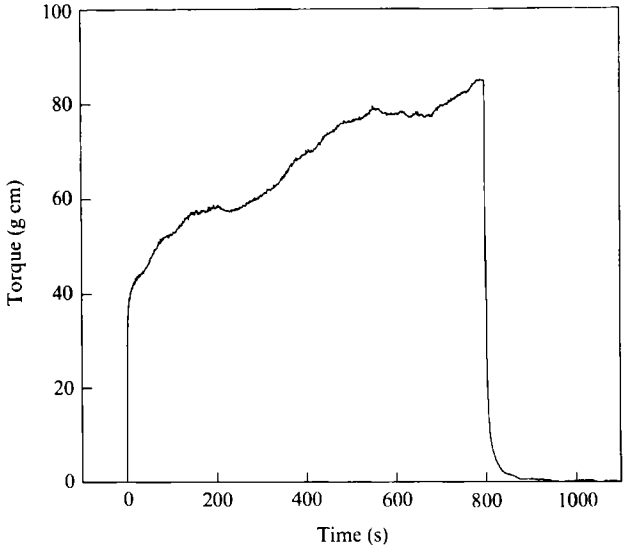

FIGURE 22. The torque as a function of time for the Taylor–Couette flow of the 6000 p.p.m. solution. The shear rate $\dot{\gamma}$ was zero for times $t < 0$ and was $\dot{\gamma} = 1.4\ \mathrm{s}^{-1}$ for $0 < t < 800$ s.

could not be accurately resolved for the more concentrated solutions since this would have required that (i) the entire system (temperature controller, motor speed, transducer) be stable for very long times relative to the period of oscillation, and (ii) the fluid sample be sheared for very long times, introducing the potential for shear degradation. The absence of a clear torque oscillation in the latter three of these figures may also be due in part to the fact that, as the critical shear rate decreased with increasing concentration, it became somewhat more difficult experimentally to access shear rates that were only marginally above the critical value.

6. Conclusions

To conclude we shall present a summary of the major predictions of the present research together with our supporting experiments. Our theoretical analysis of the elastic Taylor–Couette instability in §§1–4 demonstrated two important effects of fluid rheology: that negative second normal stresses were stabilizing, especially for very small gap ratios; and that increasing the solvent's relative contribution to the viscosity was a stabilizing influence. Table 2 presents a comparison of the critical data measured for flow of the PS/PS/DOP fluids and the predictions of the linear theory. Because the second normal stresses were found experimentally to be vanishingly small for these fluids, our rheological models and analysis predict that increasing the polymer concentration only decreases the dimensionless parameter S and thus decreases the critical Deborah number. This is qualitatively reflected in the experimental measurements. However, the theoretical predictions are, in general, overpredictions of the critical Deborah number, with the largest overprediction being approximately 25%. Clearly more data need to be accumulated before more general conclusions can be drawn; however, we further note that in our comparison with the data from our previous experiments on the PIB fluids (cf. figure 10), we again found an overprediction of the measured data for gap ratios of approximately 0.1. For the PIB fluid, as the gap ratio was increased the critical modified Deborah

number increased and the agreement between data and theory became better. Thus, in both sets of experiments the qualitative trends in the data are in agreement with the theoretical predictions, but the theory tends to overpredict the critical conditions. No explanation for this overprediction is offered at this time, although two obvious possibilities lie in our oversimplifying the time response of these elastic fluids in our rheological models and in our neglecting the development of subcritical disturbances. The former requires that we investigate fluids which are modelled via a spectrum of timescales and the latter requires a nonlinear analysis. At the present time, we are actively investigating the effects of including a spectrum of fluid relaxation times in our stability predictions (see Larson *et al.* 1991).

Although increasing the polymer concentration in our PS/PS/DOP fluids destabilized the flow, clearly there exists a possible dual role for a concentration increase since we demonstrated in §3 that the presence of second normal stress differences which are negative (and which are usually associated with entanglement effects at higher concentrations) would stabilize the flow. Thus the fact that the polymer concentration in these experiments is still small enough that there are no measurable second normal stress differences seems to be very important for the subsequent destabilization. In this context, we demonstrated that the stabilization found in our experiments using PIB fluids at small gap ratios could be explained by small negative second normal stress differences. We anticipate, therefore, that if we continue to increase polymer concentration, the flow of PS/PS/DOP fluids will strongly stabilize. We have previously alluded to the fact that the elastic Taylor–Couette instability has never been reported in more concentrated solutions even though there has been a host of such experimental work. This is consistent with such a stabilization due to a second normal stress difference.

Although we have had some success in predicting the critical conditions for the elastic instability in Taylor–Couette flow over a range of polymer concentrations and for two completely different Boger fluids, we have not made any direct measurement of the flow structure following transition. Thus, we have not been able to determine whether the linear analysis can predict the resulting flow field. These predictions of flow structure comprise a significant part of the work contained in this publication, and we look forward to experimentally evaluating the flow structure which we have visualized in our previous publications. Note that we have measured the frequency of the oscillations in the measured torque signal following the transition which occurred in our 1000 p.p.m. PS/PS/DOP solution. The measured period of these oscillations was approximately 33 s and compares favourably with the period of the oscillations of the flow streamlines predicted by the linear analysis to be 28.8 s. We note that, although far from a confirmation of the flow structure, this result nevertheless points strongly to flow oscillations at a timescale comparable to the relaxation time characteristic of the fluid, since all other timescales of the experiment were far removed from the measured period.

In summary, although a limited part of the theoretical results presented herein have been found to agree qualitatively with experimental results, clearly a more thorough experimental investigation is necessary in order to determine even the salient features of the instability flow structure. It is hoped that the present publication will spur other such investigations.

Appendix. Linear structure of the purely elastic transition in the small-gap limit

We begin by further analysing the solutions of the stability eigenvalue problem which we derived in II and included in (2.3) which governs the evolution of small disturbances in the inertialess Taylor–Couette flow of an Oldroyd-B fluid, viz.

$$U''''-2\alpha^2U''+\alpha^4U+\alpha^3\Lambda U'=0, \qquad U=U'=0, \quad x=0,1. \qquad (\text{A } 1a, b)$$

The primes refer to derivatives with respect to the gap variable x, U is the amplitude of the radial component of the disturbance velocity (cf. (2.1) and (2.2)), α is the wavenumber, and the eigenvalue, Λ, is related to the important dimensionless variables via the expression

$$\Lambda = 2(De)^2\frac{\epsilon D^2(1+2D)(D+S)-D^3(1+D)}{\alpha(D+S)^2}, \quad D=(1-\mathrm{i}\omega)^{-1}. \qquad (\text{A } 2a, b)$$

In (A 2) the Deborah number, $De=\dot{\gamma}\lambda$, where $\dot{\gamma}$ is the constant shear rate across the gap (in the small-gap limit) and $S=\eta_s/\eta_p$, where S is the ratio of solvent to polymer viscosity in the fluid. Equations (A 1) and (A 2) have been made dimensionless as discussed in §2.

We demonstrated previously in II that there are an infinite series of complex conjugate eigenvalue solutions of (A 1) all of which are purely imaginary. The consequences of this for the stability of the system were discussed at the time but the values of the complex frequency ω and their relation to the values of Λ was not detailed. For the Maxwell fluid ($S=0$), we have directly

$$\Lambda=\frac{2\epsilon(De)^2}{\alpha(1-\mathrm{i}\omega)^2}, \qquad (\text{A } 3)$$

from which it follows that there are four modes for any given set of conditions; two corresponding to each of the complex-conjugate pair $\pm\mathrm{i}|\Lambda_n|$. These eigenvalues are conveniently divided into pairs, one pair of which can never grow in time (always decaying) while the other pair grows beyond a condition defined in our previous work, viz.

$$\frac{\epsilon(De)^2}{\alpha|\Lambda_n(\alpha)|}\geqslant 1.$$

Thus, the critical condition and critical modes are defined in terms of the eigenvalues of smallest absolute magnitude which we represent by $\Lambda_1(\alpha)$. Introducing $\sigma=-\mathrm{i}\omega$, whose real part is the characteristic growth rate of the wave and whose imaginary part is the characteristic oscillation frequency, then one of the critical growing modes is defined by

$$\sigma_G=\left\{\left[-1+\left(\epsilon\frac{De^2}{\alpha\Lambda_1}\right)^{\frac{1}{2}}\right],\left(\epsilon\frac{De^2}{\alpha\Lambda_1}\right)^{\frac{1}{2}}\right\}, \qquad (\text{A } 4a)$$

and another is defined by the conjugate, σ_G^*. Similarly, σ_D and σ_D^* are decaying modes corresponding to the conjugate eigenvalue pair $\pm\Lambda_1$, where

$$\sigma_D=\left\{\left[-1-\left(\epsilon\frac{De^2}{\alpha\Lambda_1}\right)^{\frac{1}{2}}\right],\left(\epsilon\frac{De^2}{\alpha\Lambda_1}\right)^{\frac{1}{2}}\right\}. \qquad (\text{A } 4b)$$

The presence of two growing modes σ_G and σ_G^* in this system then introduces the question of structure selection present in symmetric systems subject to a Hopf-type or oscillatory bifurcation. If we restrict ourselves to only the critical mode (a restriction to which we shall return in due course) then these two modes represent travelling waves which move in opposite directions along the length of the coaxial cylinders. The eigenfunctions corresponding to the two growing modes contain a number of special relationships which can easily be demonstrated by inspection of (A 1) above. For example, if we denote one of these solutions U_G then it is easy to demonstrate that the other eigensolution is its complex conjugate, U_G^*. In addition, it is not difficult to show the following:

$$U_G(x) = U_G^*(-x), \quad U_G(x;\alpha) = U_G^*(x;-\alpha),$$
$$\mathrm{Re}\,(U_G) \Rightarrow \text{even}, \quad \mathrm{Im}\,(U_G) \Rightarrow \text{odd}.$$

The complex stream function corresponding to the approximately two-dimensional disturbance flow in the (z,x)-plane is as defined in (2.4), viz.

$$\Psi = \psi(x)\exp[\mathrm{i}(\alpha z - \omega t)], \quad \psi = \mathrm{i}U/\alpha. \tag{A 5a, b}$$

Thus, (A 1) could apply equally well to the stream function for flow in the (x,z)-plane.

The mathematical expression for the stream function corresponding to one of the critical growing modes is

$$-\alpha\Psi_u^r = U_G^i\cos(\alpha z - \omega^r t) + U_G^r\sin(\alpha z - \omega^r t) \tag{A 6a}$$
$$= U_G^i\cos 2\pi(Z-\tau) + U_G^r\sin 2\pi(Z-\tau), \tag{A 6b}$$

where the superscripts 'r' and 'i' refer to the real and imaginary parts respectively. The subscript 'u' refers to the fact that the vortices which compose this mode are tilted 'upward' along the inner cylinder and they move upward as the mode propagates.

If we assume that, rather than one of the possible travelling mode structures, the system chooses the possible standing wave structure, then the two equivalent critical modes will be present equally, and the resulting stream function will be produced by the sum of the two eigenfunctions. The real stream function for this standing wave pattern is given by the expression

$$-\alpha\Psi^r = U_G^i\cos 2\pi(Z-\tau) + U_G^r\sin 2\pi(Z-\tau) - U_G^i\cos 2\pi(Z+\tau) + U_G^r\sin 2\pi(Z+\tau). \tag{A 7}$$

The structure consists of radially propagating vortices as shown in figure 3 and discussed in §2.

Since the standing wave structure does not propagate, the question arises as to whether travelling modes could be seen in the elastic Taylor–Couette system at zero Reynolds number. To partially investigate this question, one asks whether the instability (i.e. either of the growing modes) is convective or absolute (Huerre & Monkewitz 1985). In the former case, one could presumably see travelling wave solutions under certain circumstances. In the latter case, the instability would appear to spread from the initial perturbation(s) since under these circumstances the group velocity of a small wave packet centred around the most highly amplified wave would be zero. However, depending on the reflection of modes from the ends it is possible to still see travelling modes, and one then has to analyse the instability development in finite devices.

In II, we have demonstrated for the Maxwell fluid that for the two most unstable

growing modes, the real frequency, ω^r, is related to the imaginary frequency, ω^i, through the expression, $\omega^r = \pm(\omega^i + 1)$. Thus, it is clear that

$$\left(\frac{\partial \omega^r}{\partial \alpha}\right)_{\alpha=\alpha_{max}} = \left(\frac{\partial \omega^i}{\partial \alpha}\right)_{\alpha=\alpha_{max}} = 0, \tag{A 8}$$

where α_{max} is defined as the wavenumber of largest wave growth. Equation (A 8) demonstrates that the group velocity of a packet surrounding the most highly amplified mode is zero and thus the instability (at least for the Maxwell fluid) is an absolute one. Numerical studies confirm that this is also the case for the Oldroyd-B fluid, for all values of S studied.

All of the discussion above describes the solution space for the eigenvalues and solutions for the small-gap limiting eigenvalue problem. In §3, we considered the effects of finite gap ratio, and it is interesting to discuss the change in this space as the gap ratio is increased. First, for all of our calculations involving the Oldroyd-B equations at any gap ratio, we find that there exist an infinite series of eigenmodes. These modes can be ordered in the same manner as indicated in our discussion surrounding (A 4), namely there exists an infinite series of groups of four modes. Of these four modes, two are decaying and two are growing. In addition, each of these constituent two-mode pairs is defined by complex-conjugate values of σ (cf. (A 4)). Finally, there exists a one-to-one correspondence between each of these four-mode groups and a similar four-mode set obtained from the solution of the small-gap problem (A 1). In the limit of vanishingly small gap ratio, these two sets become identical. Numerical searches of the complex plane (which involve finding the lines of vanishing real and imaginary parts of the relevant complex determinant and then searching for zero crossings) yielded no other eigenmodes.

Finally, we should mention that for finite-gap flows, the relationship between the stream function and U for any mode changes slightly. For example, the expression for the stream function of the standing wave for finite gap corresponding to the small-gap limiting equation (A 7) is

$$\begin{aligned} -\alpha \Psi^r = (1+\epsilon x)[U_G^i \cos 2\pi(Z-\tau) + U_G^r \sin 2\pi(Z-\tau)] \\ + (1+\epsilon x)[-U_G^i \cos 2\pi(Z+\tau) + U_G^r \sin 2\pi(Z+\tau)], \end{aligned} \tag{A 9}$$

where the added factors of $1+\epsilon x$ come from the finite curvature of the coordinates when the gap ratio is not vanishingly small.

REFERENCES

Berry, G. C. 1967 Thermodynamic and conformation properties of polystyrene. II. Intrinsic viscosity studies on dilute solutions of linear polystyrenes. *J. Chem. Phys.* **46**, 1338–1352.

Boger, D. V. 1977/78 A highly elastic constant-viscosity fluid. *J. Non-Newtonian Fluid Mech.* **3**, 87–91.

Drazin, P. G. & Reid, W. H. 1981 *Hydrodynamic Stability*. Cambridge University Press.

Giesekus, H. 1966 Zur stabilitat von stromungen viskoelastischer Flussigkeiten. *Rheol. Acta* **5**, 239–252.

Giesekus, H. 1972 On instabilities in Poiseuille and Couette flows of viscoelastic fluids. *Prog. Heat Mass Transfer* **5**, 187–193.

Ginn, R. F. & Denn, M. M. 1969 Rotational stability in viscoelastic liquids. *AIChE J.* **15**, 450–454.

Huerre, P. & Monkewitz, P. A. 1985 Absolute and convective instabilities in free shear layers. *J. Fluid Mech.* **159**, 151–168.

KEENTOK, M., GEORGESCU, A. G., SHERWOOD, A. A. & TANNER, R. I. 1980 The measurement of the second normal stress difference for some polymer solutions. *J. Non-Newtonian Fluid Mech.* **6**, 303–324.

LARSON, R. G. 1988 *Constitutive Equations for Polymer Melts and Solutions*, pp. 33, 120–121, 136. Butterworths.

LARSON, R. G., MULLER, S. J. & SHAQFEH, E. S. G. 1991 The elastic Taylor–Couette instability for rheologically complex fluids. *J. Non-Newtonian Fluid Mech.* (to be submitted).

LARSON, R. G., SHAQFEH, E. S. G. & MULLER, S. J. 1990 A purely viscoelastic instability in Taylor–Couette flow. *J. Fluid Mech.* **218**, 573–600 (referred to herein as II).

LAUN, H. M. & HINGMANN, R. 1990 Rheological characterization of the fluid M1 and of its components. *J. Non-Newtonian Fluid Mech.* **35**, 137–157.

LEE, C. S., MAGDA, J. J., MULLER, S. J. & LARSON, R. G. 1991 Dependence of 2nd normal stress differences on polymer concentration. *Natl AIChE Meeting, Session on Advances in Rheology* (Abstract Submitted).

MAGDA, J. J., LOU, J., BACK, S. G. & DEVRIES, K. L. 1991 The second normal stress difference of a Boger fluid. *Polymer* (to appear).

MULLER, S. J., LARSON, R. G. & SHAQFEH, E. S. G. 1989 A purely elastic transition in Taylor–Couette flow. *Rheol. Acta*, **28**, 499–503 (referred to herein as I).

NORTHEY, P., ARMSTRONG, R. C. & BROWN, R. A. 1990 Finite-element calculation of purely elastic, nonlinear transitions in circular Couette flow. *Paper* 167j, *Annual AIChE Meeting, November, 1990.*

NORTHEY, P., BROWN, R. A. & ARMSTRONG, R. C. 1989 Numerical calculation of time-dependent, two-dimensional inertial flows described by a multimode UCM model, *Paper* 166Adb, *Annual AIChE Meeting, November, 1989.*

QUINZANI, L. M., MCKINLEY, G. H., BROWN, R. A. & ARMSTRONG, R. C. 1991 Modeling the rheology of polyisobutylene solutions. *J. Rheol.* **34**, 705–748.

TAYLOR, G. I. 1923 Stability of a viscous liquid contained between two rotating cylinder. *Phil. Trans. R. Soc. Lond.* A **223**, 289–343.